Tectonophysics 700–701 (2017) 108–130

Contents lists available at ScienceDirect

Tectonophysics

journal homepage: www.elsevier.com/locate/tecto

Variations in fault-slip data and cooling history reveal corridor of heterogeneous backarc extension in the eastern Aegean Sea region

Uwe Ring [a,*], Klaus Gessner [b], Stuart Thomson [c]

[a] Department of Geological Sciences, Stockholm University, 10691 Stockholm, Sweden
[b] Centre for Exploration Targeting, The University of Western Australia, Crawley 6009, Australia
[c] Department of Geosciences, University of Arizona, Tucson, AZ, USA

ARTICLE INFO

Article history:
Received 18 October 2016
Received in revised form 10 February 2017
Accepted 13 February 2017
Available online 20 February 2017

Keywords:
Fault-slip data
Heterogeneous deformation
Plate boundary structures
Anatolia
Aegean Sea region

ABSTRACT

We report fault-slip data across the boundary between the highly extended and largely submerged crust underlying the Aegean Sea from Samos in the north to eastern Crete in the south, and the much less extended and emergent crust of western Anatolia. We identify three brittle deformation increments, a late Miocene (mainly Pliocene) to Recent crustal stretching increment, an intermittent early to late Miocene shortening increment concurrent with extension and magmatism, and a Miocene extensional event. The youngest increment documents late Miocene to Recent NNE extension over large areas, but can locally also be oriented SE (Amorgos and Astipalea Islands), and ESE (eastern Crete) suggesting overall oblate strain geometry. The intermittent Miocene (~24–5 Ma) fault-slip records suggest overall prolate strain geometry, where NNE stretching is accompanied by E–W shortening. The older extension event is mainly NNE directed but on Samos Island extension is E–W, probably reflecting local extension in a sinistral wrench corridor in the early/mid Miocene. Overall it seems that since the early Miocene NNE-trending extension is the dominant regime in the eastern Aegean with an intermittent component of short-lived E–W shortening. The existence of a corridor of heterogeneous crustal deformation – which is spatially associated with uncharacteristically old fission track ages – and the apparent change in strain geometry in time challenge concepts that propose that the eastern Aegean Sea and western Anatolia have been deformed as a continuous tectonic domain since the Miocene. We propose that the regional variation in extensional strain geometry resulted from a sinistral wrench component that was superimposed on the regional 'background' NNE extension by translation across a diffuse plate boundary. We conclude that the eastern shoreline of the Aegean Sea is controlled by a Miocene to Recent sinistral wrench corridor that accommodated movement between different lithospheric domains.

1. Introduction

The Aegean Sea forms a narrow, complexly shaped continental extensional basin above the SSW-ward retreating Hellenic subduction zone. It is bordered to the west, north and east by the Eurasian mainland (Fig. 1) indicating that extension and basin formation occurred heterogeneously across the region. Whereas the western shoreline of the Aegean Sea can be explained by eastward-increasing crustal thinning forced by the SSW-ward retreat of the Hellenic subduction system, the first order tectonic control on its eastern shoreline is not well understood.

Global Positioning System (GPS) based geodetic analysis of deformation using a ~100 year old triangulation network that has been reoccupied, allows, together with earthquake data, the reconstruction of the recent velocity field (Billiris et al., 1991; Kiratzi and Papazachos, 1995; Davies et al., 1997; Kahle et al., 1999; Ganas et al., 2005; Ganas and Parsons, 2009; Özeren and Holt, 2010; Aktug et al., 2009). Fault-slip data reported by Angelier et al. (1982), Mercier et al. (1987) and Ring et al. (2001, 2011), however, suggest that, in places, young (Quaternary) extension directions vary by up to 70° from kinematics implied by geodetic and focal mechanism data. This discrepancy raises at least two questions: (1) how precise do recent velocity fields match crustal deformation and, (2) how far back can velocity fields derived from geodetic measurements and focal mechanisms be extrapolated back in time in a meaningful way.

We present a large data set of new fault-slip data measured on striated and corrugated fault planes. The youngest data set is from faults that control the topography and are in part seismically active. We compare the results of our fault-slip analysis with extension directions constrained by GPS and focal mechanisms, and maps of apatite and zircon fission track ages. Our study area straddles the boundary between the Aegean Sea basin and the adjacent Anatolian mainland (Fig. 1), a region that based on their geodetic data McClusky et al. (2000) consider a

* Corresponding author.
E-mail address: uwe.ring@geo.su.se (U. Ring).

http://dx.doi.org/10.1016/j.tecto.2017.02.013
0040-1951/

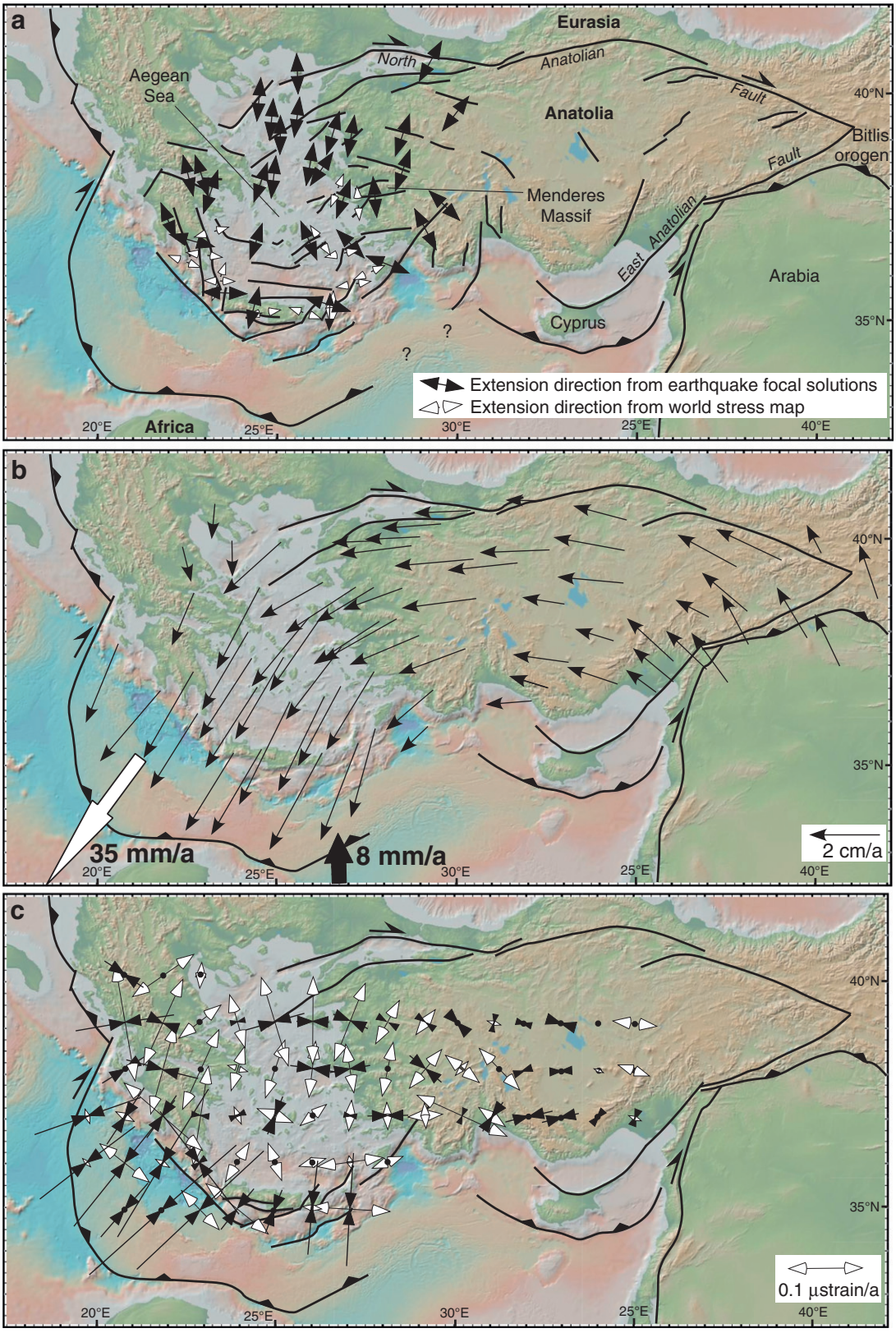

Fig. 1. (a) Simplified tectonic map of eastern Mediterranean superimposed on topography and bathymetry (GeoMapApp, Ryan et al., 2009); selected current extension directions from earthquake focal solutions (Kahle et al., 1999) and world stress map (www.world-stress-map.org) showing NNE directed extension in northern and central Aegean and mix of N–S and radial extension in southern Aegean. (b) GPS-derived horizontal velocities (Kahle et al., 1999; McClusky et al., 2000; Aktug et al., 2009) in Eurasia-fixed reference frame; especially magnitudes of GPS velocities show that pattern controlled by SW-ward retreat of Hellenic slab; big black arrow shows motion vector of Africa relative to Eurasia, big white arrow shows maximum motion of Aegean microplate relative to European reference system (from Kahle et al., 1999). (c) Principal values and axes of strain rates calculated from velocity field shown in (b), white arrows indicate extension; black arrows shortening, dots indicate low strain rates; data show radial shortening in outer Hellenic arc (from Kahle et al., 1999).

diffuse plate-boundary zone between Aegea and Anatolia. Ring et al. (1999), Govers and Wortel (2005), Gessner et al. (2013) and Jolivet et al. (2015) argue for a sinistral wrench corridor along the west coast of Anatolia, where differential extension between Aegea and Anatolia dates back to the early Miocene. We first show that the Aegea-Anatolia plate-boundary zone spatially coincides with a corridor of old zircon and apatite fission-track ages. We then compare the fault-slip derived strain axes with those from geodetic and focal plane work. These data will help to fill gaps in the data base along the Aegea-Anatolia plate boundary zone, for instance the differing Quaternary to recent extension directions or issues with extension rates in the Menderes Massif (see below). The motivation for putting this paper together is that we believe that there is a need for more robust field data that may help to design and perform better constrained models for how complexly extending regions in convergent settings evolve in space and time.

2. Tectonic setting

The tectonics of the eastern Mediterranean is driven by the convergence between Africa and Eurasia along the Hellenic and Cyprus subduction zones, and the Bitlis orogen (Fig. 1). The complex plate tectonic pattern also involves a number of microplates. The two important microplates relevant for this paper are the Anatolian and Aegean microplates (McClusky et al., 2000). The boundary between these two microplates is diffuse and poorly defined and in part coincides with the ill-defined connection between the Hellenic and Cyprus subduction zones. At shallow levels of the lithosphere this diffuse plate-boundary zone probably accommodates rapid southwestward motion of the Aegean block relative to Anatolia, caused by a tear between the rapidly sinking Hellenic slab and its poorly constrained Anatolian counterpart (Barka and Reilinger, 1997; de Boorder et al., 1999; Ring et al., 1999; Govers and Wortel, 2005; Gessner et al., 2013; Jolivet et al., 2015).

The collision of the Arabian and Eurasian plates along the Bitlis orogen is generally thought to control the westward displacement of a coherent Anatolian microplate. The onset of this 'escape' of Anatolia along the North and East Anatolian faults is usually placed at 13–11 Ma in the east, with westward propagation into the north Aegean region having occurred by 5–3 Ma (Barka, 1992; Şengör et al., 2008). The escape hypothesis works well with today's geodetic data, but this does not necessarily mean that it can be assumed to take these kinematics back in time to 13–11 Ma. Field data from various areas along the North Anatolian Fault show Late Cretaceous collision and subsequent extensional and strike-slip deformation in central Anatolia (Şengör and Yilmaz, 1981), Eocene collision in western Anatolia and subsequent Miocene extension (Şengör et al., 1984; Ring et al., 2007a; Gessner et al., 2013), and late Miocene collision in east Anatolia (Şengör and Yilmaz, 1981; Şengör et al., 2003). Subduction zone retreat in the Aegean since ~23 Ma provided the space and thus facilitated extrusion of western Anatolia (Le Pichon et al., 1995; Le Pichon and Kreemer, 2010). It thus appears more conceivable that a feature as big as the North Anatolian Fault is a complex, long-lived structure that formed during multiple events over a prolonged period of time. We envisage that a number of pre-existing fault segments linked up as a result of various collisions across Anatolia and subduction zone retreat in the Aegean. The key question then is when all the segments finally linked up to form the present day North Anatolian Fault and whether this occurred during escape of Anatolia following continental collision in the Bitlis orogen.

The velocity of the escaping Anatolian plate relative to stable Eurasia increases westward (Le Pichon et al., 1995; Reilinger et al., 1997, 2006; McClusky et al., 2000; Aktug et al., 2009). The leading edge of the African plate is being subducted along the Hellenic subduction zone at a higher rate (~35 km Ma^{-1}) than the overall convergence rate between the African and Eurasian plates of ~8 km Ma^{-1}) (Fig. 1b), requiring that the subduction zone moves SSW-ward relative to Eurasia (Royden, 1993). This retreat of the subducting African plate and the westward escape of Anatolia control the current velocity field in the Aegean (Le Pichon et al., 1995; Pérouse et al., 2012). Scaled mechanical, as well as numerical experiments suggest that the crustal velocity field is caused by a combination of toroidal asthenospheric flow around the retreating slab and differences in gravitational potential energy across Anatolia (Kincaid and Griffiths, 2004; Piromallo et al., 2006; Le Pichon and Kreemer, 2010; Özeren and Holt, 2010).

The Aegean Sea is underlain by thin and hot crust (Sodoudi et al., 2006). However, crustal thinning in the southern Aegean Sea preceded the formation of the present North Anatolian Fault leaving the southern Aegean as a thin, rigid, coherent block that translates towards the Hellenic subduction trench from ~5–3 Ma onwards (McClusky et al., 2000). The compilation of earthquake data by Kiratzi and Louvari (2003) corroborates that the southern Aegean block is hardly deforming and the few earthquakes there seem to be restricted to the vicinity of the volcanic arc.

Jackson and McKenzie (1988) proposed that the Aegean plate moves with a distinctly different velocity than the Anatolian plate. McClusky et al. (2000) showed that this differential motion is distributed across western Turkey by a zone of N–S extension (Fig. 1), for which they estimated an extension rate of 10–15 km Ma^{-1}. The main late Miocene to Recent extension structure in west Turkey is the Central Menderes core complex with the associated Gediz, Büyük and Kücük Menderes graben (Fig. 2). For this extensional system Gessner et al. (2001) and Ring et al. (2003a) estimated an extension rate of ~2 km Ma^{-1} since ~5 Ma, similar to the geodectic velocity field analysis by Aktug et al. (2009). Thomson and Ring (2006) showed that the active Simav graben further north is extending at a rate of <1 km Ma^{-1} since the last few million years. Overall, calculated displacement rates of the major extensional structures in western Turkey fall short by a factor of at least three compared to the GPS derived rates, probably because rather than segmenting into distinct crustal blocks, the entire continental lithosphere is thinning homogeneously (Aktug et al., 2009) since the late Miocene onset of stage 2 metamorphic core complex formation (Gessner et al., 2013).

The GPS-derived recent velocity field shows, in an Anatolia-fixed reference frame, radial motion in the southern Aegean (McClusky et al., 2000). This fits well with recent numerical models for convergence of lateral heterogeneous lithosphere (Duretz et al., 2014; Moresi et al., 2015). The extension axes of earthquakes in the southern Aegean are, in general, radial to the arc and aligned down-dip within the subducting slab (Benetatos et al., 2004). Another important group of earthquakes occurs within the overriding Aegean crust and is not directly concerned with accommodating Africa-Aegea convergence. These earthquakes represent E–W extension, mostly on N–S normal faults, and are generally shallower than 20 km. Their orientations contrast with the generally E–W striking normal faulting events that characterize the N–S extension of the central and northern Aegean, western Turkey and mainland Greece (McKenzie, 1978).

3. Fission-track age maps

Fission-track age maps for zircon and apatite constrain cooling in the upper crust and are thus intimately related to brittle faulting. Zircon fission-track (ZFT) ages for rapidly cooling rocks provide an approximation for the arrival of the exhuming rocks in the brittle crust (Brix et al., 2002; Reiners and Brandon, 2006) and are thus an important constraint for dating the onset of brittle deformation. Fission-track age maps have been published for the central and southern Aegean Sea by Ring et al. (2010) and apatite fission-track (AFT) cooling maps for large parts of the Anatolide Belt by Gessner et al. (2001, 2013) and Ring et al. (2003a). Here we present an extended data set for the entire Hellenide-Anatolide Orogen from the western Aegean Sea region to the eastern Anatolide Belt (Fig. 3).

The regional pattern of AFT ages (closure temperature of ~80–120 °C; Reiners and Brandon, 2006) (Fig. 3a) shows a prominent belt of young ages (~14–8 Ma) running in an ENE direction from the

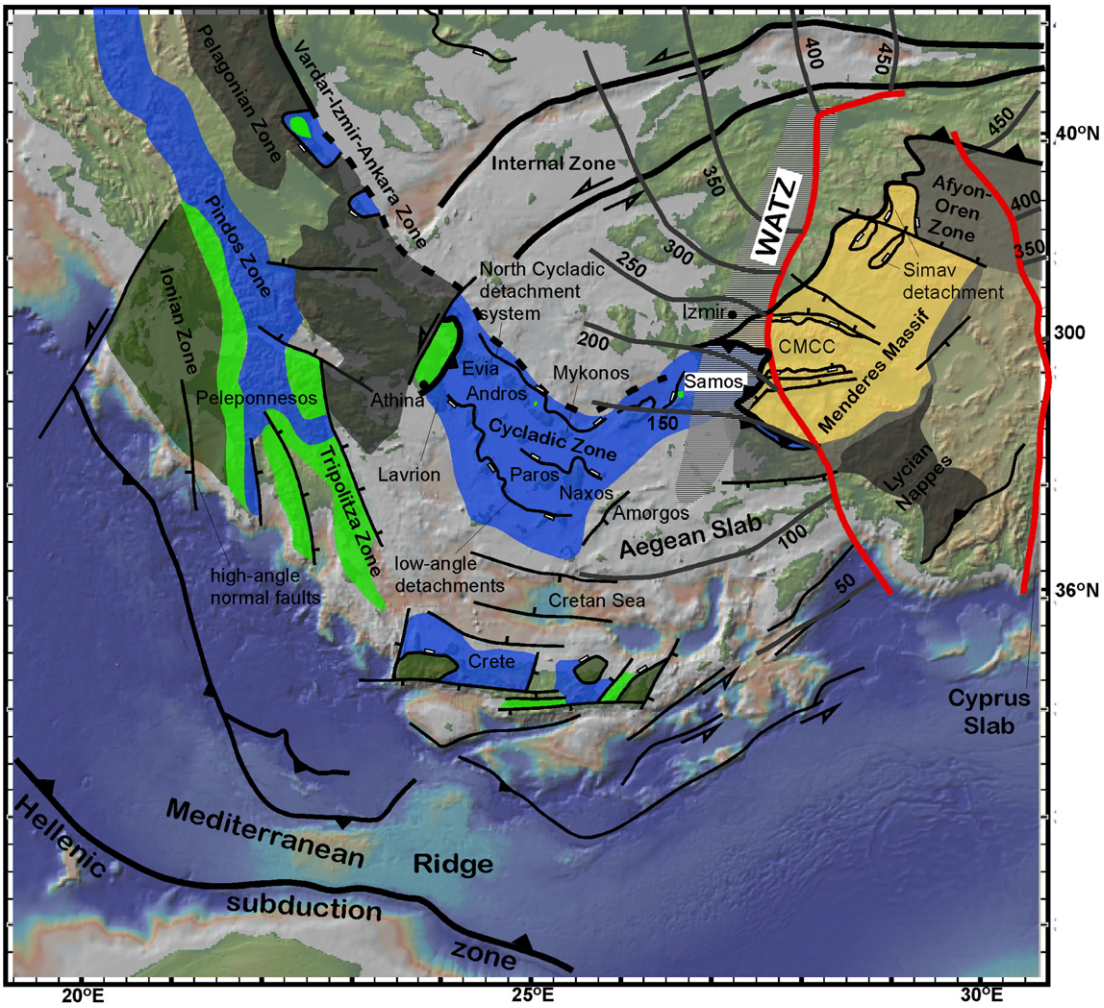

Fig. 2. Tectonic map of Aegean Sea and west Anatolia showing Hellenic subduction zone, main tectonic zones, major thrusts, faults and low-angle extensional detachments. Superimposed on map is projection of upper limit of Aegean and Cyprus slab fragments (Berk Biryol et al., 2011; Gessner et al., 2013) with slab contours (in km, grey heavy lines) showing c. 300 km wide asthenospheric mantle domain beneath Menderes Massif (in between bold red lines), and large lithospheric-scale transfer zones west of mantle window (West Anatolia Transfer Zone, WATZ, of Gessner et al., 2013), which largely coincides with Aegea-Anatolia plate boundary of McClusky et al. (2000). Also shown Central Menderes core complex (CMCC) with Gediz (north) and Kücük Menderes (south) graben, Simav detachment and localities mentioned in text. (For interpretation of the references to color in this figure legend, the reader is referred to the web version of this article.)

southern Peleponnesus into the central Anatolide Belt. The young AFT ages define a broad region in the central Aegean and a distinctly smaller patch in the central Menderes Massif. Old ages of >25 Ma occur in the south and southeast Aegean, along the west Anatolian coastline and in the northern Menderes Massif. Overall, the cluster of older ages in the Menderes Massif and the SW Turkish coastline occur at the same latitude as the cluster of young Miocene AFT ages in the central Aegean suggesting a left-lateral offset of the region of younger Miocene cooling somewhere between the eastern Aegean Sea and western Anatolia.

The ZFT map (closure temperature of 200–260 °C for radiation-damaged zircon; Reiners and Brandon, 2006) (Fig. 3b) is, in general, similar to the pattern of AFT ages by also showing an ENE-trending belt of young ages in the central Aegean that is left-laterally offset relative to the youngest ZFT ages in western Anatolia. Furthermore, the map shows unreset or only partially reset ages, i.e. older than 45 Ma, in the southeast Hellenide-Anatolide Orogen (eastern Crete, Amorgos Island and westernmost part of SW Turkey) at the same latitude as Miocene ZFT cooling ages in the central Aegean. Older ZFT ages also occur in the hangingwall of the Simav detachment in the northern part of west Turkey (reset during earlier Cretaceous high-pressure metamorphism).

Overall, the central Aegean Sea region from the Cyclades to the Cretan Sea basin is characterized by young Miocene (~14–8 Ma) ZFT and AFT ages attesting to a prominent phase of extensional deformation and associated footwall cooling at this time. Young FT ages in the Menderes Massif are confined to a rather small area in the Central Menderes core complex, where AFT ages are as young as 1.6 Ma (Gessner et al., 2001; Ring et al., 2003a). The young FT ages of the central Aegean occur at the same latitude as distinctly older FT ages immediately to the east in western Anatolia. There is no evidence for <15 Ma cooling in this zone of older ages, suggesting left-lateral strike-slip motion and not normal faulting since 15 Ma. This apparent left-lateral offset in FT ages seems to be more pronounced for the AFT ages, suggesting that the structures that cause the offset are associated with progressive footwall cooling and thus are a result of ongoing extensional faulting. The N–S offset of the differentially extending tectonic domains of the Aegean Sea and the Menderes Massif broadly coincides with the position of the diffuse Aegea-Anatolia plate boundary proposed by McClusky et al. (2000) and the crustal and lithospheric discontinuities advocated by Ring et al. (1999), Gessner et al. (2013) and Jolivet et al. (2015).

4. Fault-slip data: methods and approach

On Samos, Fourni, Ikaria, Patmos, Amorgos and Astipalia Islands, in eastern Crete and western Turkey we carried out detailed geologic mapping at the 1:5000 to 1:10,000 scale and mapped crosscutting

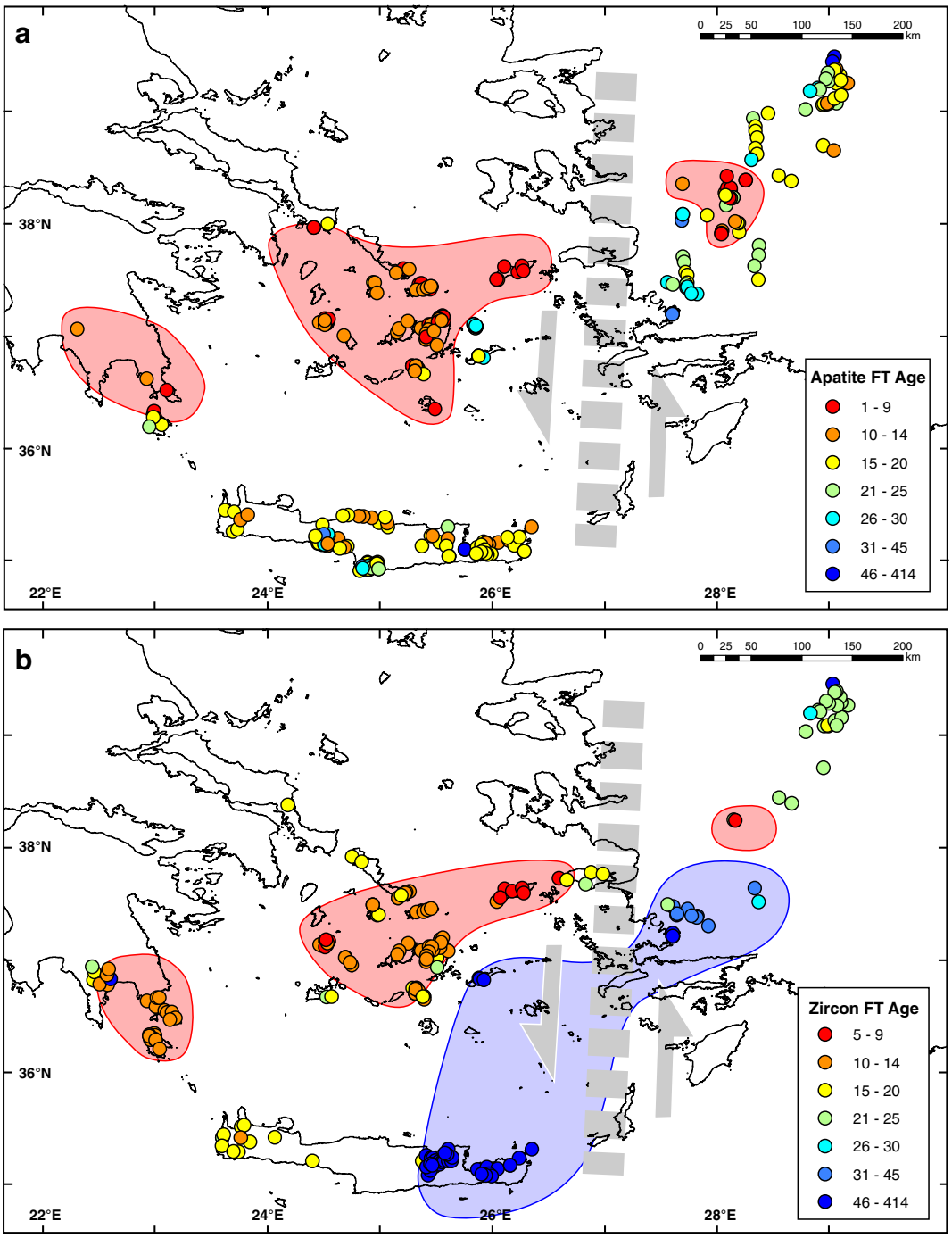

Fig. 3. (a) 249 apatite-fission track (AFT) ages from central Aegean, western Turkey and Crete coloured-coded by age; hand-drawn contours highlight young (red) age clusters. Youngest AFT ages (<14 Ma) define ENE-trending belt from Peleponnesos in west to Ikaria Island in east; similar young ages in Central Menderes core complex (CMCC in Fig. 2); old ages (>20 Ma) in western Anatolia and in southeastern Aegean Sea region. Grey, heavy-dashed line coincides with WATZ and delineates left-lateral offset of young age clusters in Aegean and west Turkey. (b) 170 zircon-fission track ages (ZFT) from central Aegean, western Turkey and Crete (contouring as in (a) with additional cluster of old (blue) ages). Clusters of young (<14 Ma, red) ZFT ages in Aegean and west Turkey separated by ages of 25–15 Ma on Samos; ZFT ages from west Anatolia significantly older than those from adjacent central Aegean and apparently sinistrally offset along WATZ. Data are from Thomson et al. (1998a, 1998b, 1999, 2009), Brix et al. (2002), Hejl et al. (2002), Brichau et al. (2006, 2007, 2008, 2010), Ring et al. (2003a, 2007a, 2007b, 2009), Kumerics et al. (2005), Marsellos and Kidd (2008), Marsellos et al. (2012), S. Thomson (unpubl. data). A full sample list can be obtained from S. Thomson. (For interpretation of the references to color in this figure legend, the reader is referred to the web version of this article.)

faults (Ring et al., 1999; Ring, 2001; Rosenbaum et al., 2007; Ring et al., in preparation). In addition, we used satellite images, earthquake data and morphologic criteria to identify the youngest fault generation. The major goal was to identify the youngest set of faults and to collect fault-slip data from these young faults. We also report data from older fault generations with the aim to better identify and constrain in time a phase of poorly understood E–W shortening that affected parts of the Cyclades and west Turkey (Ring et al., 1999; Avigad et al., 2001; Menant et al., 2013; Sümer et al., 2013).

The youngest set of faults is expressed by linear fault scarps. The faults are in general the most prominent geomorphic features causing pronounced uplift in their footwalls. Geologic constraints and (U-Th)/He ages show that throws on some of the studied faults are smaller than ~5 km corresponding to footwall uplifts of <2 km. Young fault

zones in areas of high topography are commonly diffuse and obscured by landslides. The hangingwalls of the young faults are usually filled with alluvium and slope-derived deposits.

The fault zones are characterized by fault gouge, which is usually a few decimeters thick, and/or a wider zones of intense cataclasis. The fault planes are best developed in marble and contain millimeter-scale frictional-wear striae and decimeter-scale corrugations. We have also collected fault-slip data in volcanic, ophiolitic and siliciclastic rocks in which we focused on frictional-wear striae. In the footwalls of the main fault planes are arrays of minor striated faults. The main argument for relating these minor faults to the kinematic evolution of the main faults was their spatial relationship to the main fault plane. Away from the main traces of the faults usually no minor fault planes have been observed, so that the increasing number of secondary faults in the vicinity of the main fault zones is thought to imply a genetic link between the minor faults and the main faults. Crosscutting relationships between vein-filling generations in the fault zones indicate that the minor faults formed before the main fault planes (see also Roberts and Ganas (2000) for the western Aegean). Thus, fault-slip data from the minor fault arrays provide information on the kinematics of the early stages of faulting and they do not only record the last increments of movement on the fault.

The minor fault arrays in the footwalls of the brittle fault zones are commonly segmented into a few to 10′s of centimeter big blocks whose surfaces have a variable distribution of orientations. Individual blocks are separated by thin, slickensided surfaces with fibrous striae. Sliding of the blocks past one another occurs along these surfaces and accommodates displacement in the fault zone. The direction and sense of shear on these surfaces can be deduced from the orientation of fibers and fractures associated with the fault (Petit, 1987). The orientations of fibers have been measured at the contact of the gouge zones with the country rock and not within the gouge zone itself where rotations of the fibers may have occurred. The cataclastic rocks in the vicinity of the main trace of the studied faults have a rubbly to fragmental appearance and show numerous mesoscopic brittle faults. The fault planes are characterized by anastomosing clayey and carbonate-rich gouge layers with thin (1 mm to 10 cm) zones of cataclasite, breccia and hematite- and/or clay-coated fractured rock. Bleaching and alteration of intact rock occurs in the vicinity of faults. Weakly oriented phacoid-shaped tectonic slivers of country rock within the fault zone are in the centimeter to decimeter scale. The fault surfaces contain Riedel-shears, which caused lunate and crescentic structures at their intersections with the fault plane. In a section parallel to the striation and perpendicular to the fault plane the Riedel-surfaces are characterized by fine seams of greyish-brown material. The clayey and the greyish-brown material apparently derived from the alteration of phyllosilicate, calcite/dolomite, feldspar and amphibole.

To evaluate the kinematics of the faults the orientation of primary and secondary fault and foliation planes, plunging directions of striations and the sense of relative displacement on these planes were mapped in order to determine principal strain axes (Marrett and Allmendinger, 1990). The scale of observation was usually held small (i.e. outcrop scale). Fiber orientations on slickensides are commonly simple, consistent, and are easily interpretable with the geometry of the studied fault zones at the regional scale. The displacement of the measured fault planes was generally in the centimeter to decimeter range. A simple method has been used to determine principal strain axes from these crosscutting faults and associated slickensides (program “Fault Kinematics” written by R. Allmendinger). This method graphically constructs the principal incremental shortening and extension axes for a given population of faults. Each pair of axes lies in the movement plane of the fault (i.e., a plane perpendicular to the fault plane that contains the unit vector parallel to the direction of accumulated slip, and the normal vector to the fault plane). Furthermore, each pair of axes makes angles of 45° with each of both vectors. For distinguishing between the shortening and extension axes, information on the relative sense of slip is needed. Since the method converts the measurements into a fault-plane solution, the kinematic axes of a fault portray only a different and visually more convenient presentation of the original data. Bingham distribution statistics for axial data were used to optimize clusters of kinematic axes of a fault array (Mardia, 1972).

The investigation of faults and movements on them in anisotropic, thus inhomogeneous rocks, reflects displacement versus strain relationships. Because deformation is finite and involves internal rotations, fault-slip data are fundamentally kinematic. Roberts and Ganas (2000) concluded that the results of stress inversion studies should not be used to test quantitative tectonic models. We use our fault-slip data to extract information on the orientation of extension directions instead of attempting to derive stress trajectories. These extension directions should be comparable with strain orientations derived from geodetic and focal mechanism data.

5. Results

We present fault-slip measurements from 114 outcrops in western Anatolia, the islands of Samos, Fourni, Ikaria, Patmos, Amorgos, Astipalia and eastern Crete (Fig. 1).

5.1. Western Anatolia

The extensional history of western Antolia is largely characterized by low-angle normal faulting and core complex formation (Hetzel et al., 1995; Işık and Tekeli, 2001; Gessner et al., 2001; Seyitoğlu et al., 2002; Seyitoğlu et al., 2004; Ring et al., 2003a; Ring and Collins, 2005). Ductile NNE-directed extension started at ~24 Ma in the north along the Simav detachment and ceased by about 19 Ma (Thomson and Ring, 2006). This extension created the major E–W-trending graben of west Turkey. Especially in the northern Menderes Massif the basement in the footwall of the Simav detachment is folded about NNE-trending axes which are subparallel to the extension direction and mid Miocene sediments onlap gneiss ridges in the cores of large-wavelength open folds (Purvis and Robertson, 2004, 2005). Low-temperature geochronology data indicate that a second stage of low-angle faulting commenced in the central Menderes Massif by ~5 Ma and continues today. During both phases of low-angle faulting no change in the kinematic framework occurred (Gessner et al., 2001; Ring et al., 2003a; Hetzel et al., 2013) indicating that NNE-SSW extension dominates the structural evolution in large parts of the Menderes Massif. However, in the west near the Aegean Sea coast additional NE-striking faults occur, which have strike-slip kinematics (Özkaymak et al., 2013; Sümer et al., 2013) (Fig. 1).

The youngest generation of faults is morphologically well expressed and, at least in part, seismically active (Tan et al., 2008) (Fig. 4). Fault-slip data from these fault zones show heterogeneous data sets indicating N- to NNE-directed extension (Fig. 5a–o). The shortening axes are subvertical indicating an extensional tectonic regime. Data from E–W-striking faults depict mainly conjugate or single sets of E–W-striking normal faults (Fig. 5a–e). NE-striking faults have an earlier history (see below) and the young increment shows oblique-dextral-normal kinematics (Fig. 5f–l). A third set of NE-striking faults has normal to oblique-normal kinematics (Fig. 5m–o). All data sets provide a consistent NNE-directed extension direction.

There are numerous subvertical faults subparallel to the NNE-trending extension direction. Emre and Barka (2000) showed that the Tuzla fault is an active fault, and they assign a dextral sense of displacement to it. However, Genç et al. (2001) called for left-lateral kinematics on the Tuzla fault. Our fault-slip data (Fig. 5h) show mainly dextral movement on small-scale NNE-striking faults associated with the Tuzla fault. Also the other NNE-striking subvertical faults show dextral strike-slip kinematics (Fig. 5f–l) (see also Yolsal-Çevikbilen et al., 2014) but there are also minor faults with sinistral offsets.

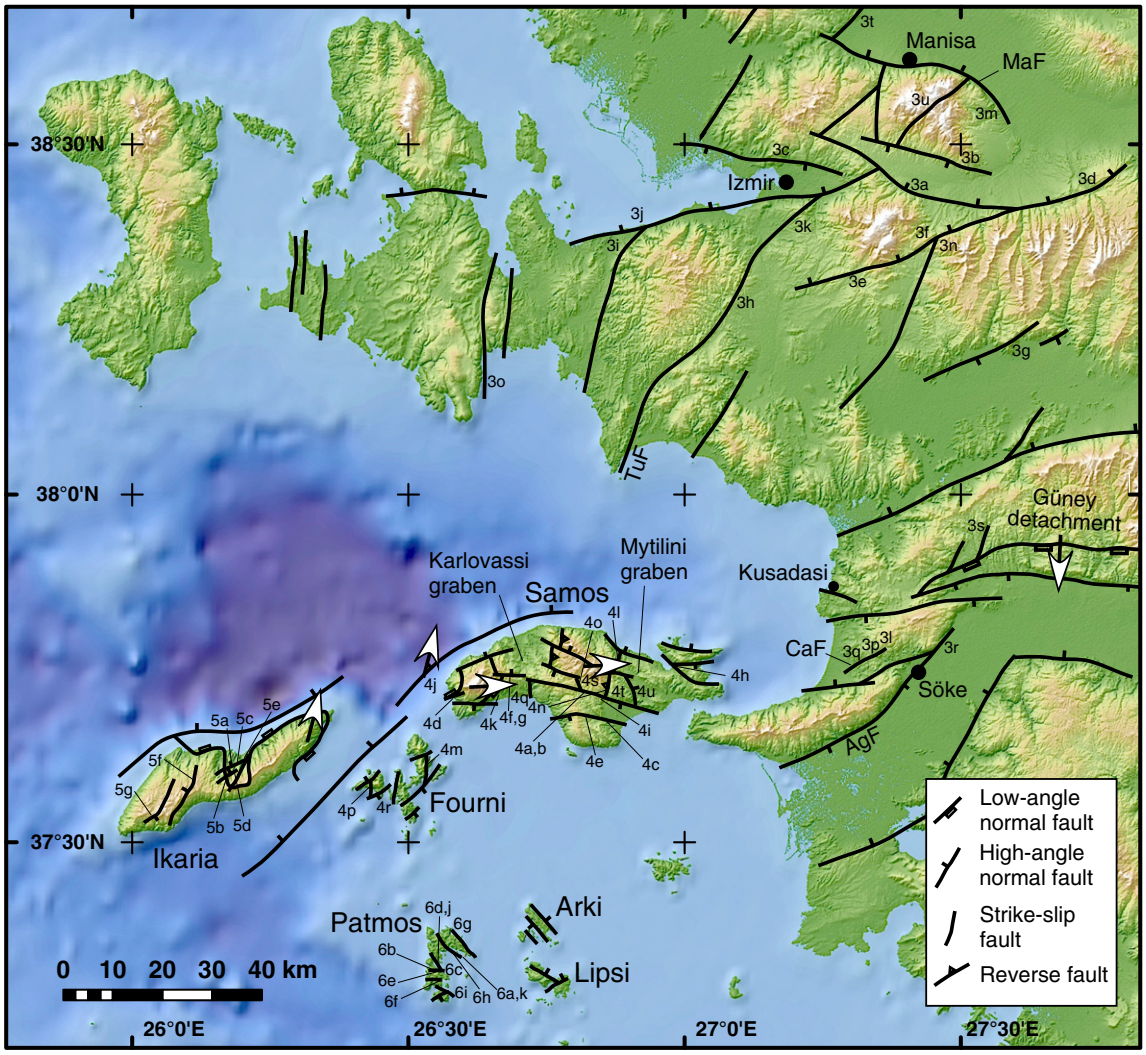

Fig. 4. Topographic map of western Anatolia and the eastern Aegean Sea showing main faults and sample localities for Figs. 5–8; TuF = Tuzla Fault; CaF = Caferli Fault, MaF = Manisa Fault, AgF = Ağaçli Fault. Mapped faults show consistent crosscutting relations. Map based on own observations and Wyers and Barton (1986), Ring et al. (1999), Kumerics et al. (2005), Uzel et al. (2012) and Sümer et al. (2013). Map base: bathymetry 90 m GMRT DEM used in GeoMapApp (Ryan et al., 2009), onland topography based on 30 m SRTM version 3 data (https://lpdaac.usgs.gov/dataset_discovery/measures/measures_products_table/srtmgl1_v003).

The topography-controlling faults crosscut or reactivate older faults. Most of these older faults strike NE and are subvertical (Fig. 4). Fault-slip data indicate a transpressional regime characterized by E–W shortening and N–S extension mainly associated with dextral, NE-striking strike-slip faults (Fig. 5p–u). The dextral strike-slip faults are cut by low-angle detachments related to the Güney and Kuzey detachments fault systems (see also Özkaymak et al., 2013 for the Kuzey detachment, and Sümer et al., 2013 for the Güney detachment) (Fig. 4).

The older set of strike-slip faults occurs in sediments with a mid to late Miocene stratigraphic age (Sümer et al., 2013; Özkaymak et al., 2013) and they are cut by the young (<~5 Ma) low-angle detachments. These constraints provide a broad age of ~12–5 Ma for transpressive deformation and E–W shortening (Mercier, 1981; Uzel et al., 2012). Sümer et al. (2013) favour an age of ~5 Ma for E–W shortening. The youngest set of normal faults is associated with low-angle detachment faulting and moved from ~5 Ma until the present (Gessner et al., 2001; Sümer et al., 2013; Özkaymak et al., 2013).

5.2. Samos and Fourni Islands

The Miocene to recent extension history of Samos and Fourni is complicated. The oldest phase of low-angle normal faulting occurred along the Selçuk and Kerketas extensional shear zones at ~20–14 Ma, was top-E directed, and associated with initial graben formation in Samos (Ring et al., 1999; Kumerics et al., 2005). The top-NNE-displacing Kallithea detachment initiated by ~10 Ma and NNE–SSW extension was later resolved on high-angle normal faults (Ring et al., 1999). NNE extension was interrupted by a short-lived phase of E–W shortening with folding and reverse faulting between 9 and 8.6 Ma (Ring et al., 1999).

The morphologically most prominent faults belong to a set of steeply dipping (55–70°) E–W to NW-striking faults that crosscut all other faults (Fig. 4). Earthquake data from these faults (Tan et al., 2014) show normal to oblique-normal faulting and N- to NE-directed extension. Based on overprinting criteria in dated sediments, Ring et al. (1999) showed that this set of normal faults formed after 8.6 Ma and that the NW-striking faults represent the youngest increment of this faulting phase. The striations and corrugations on these faults are all almost perpendicular to the fault strike indicating pure dip-slip faulting and NE-oriented extension associated with the NW-striking faults (Fig. 6a–c). Fault-slip data indicate N–S extension on the earlier E–W-striking faults (Fig. 6d–i).

The next older set consists of ~N-striking reverse faults that resulted from E–W shortening (Fig. 6j–p). Outcrops usually display simple fault sets (Fig. 6j–n), but also conjugated sets of N–S reverse faults (Fig. 4o), or heterogeneous sets (Fig. 6p) occur. Ring et al. (1999) showed that

this shortening phase also produced folds and thrusts in the Miocene sedimentary sequence and the metamorphic basement of Samos. Cross-cutting relationships indicate that this shortening phase was short-lived and occurred between 9 and 8.6 Ma (Ring et al., 1999; Ring et al., 2007a).

The oldest fault set comprises normal faults resulting from E- to NNE-directed extension (Fig. 6q–u). This fault set represents a late phase of low-angle extensional shearing on Samos Island and was responsible for initial graben formation in the Serravallian at about 14–13 Ma (Ring et al., 1999) and top-NNE emplacement of the Kallithea extensional nappe in western Samos between 10 and 9 Ma. Pe-Piper and Piper (2007) showed that the 10 Ma old monzogranite at the western end of Samos and 11–8 Ma old basalts and trachytes were probably sourced from an enriched mantle. Ring et al. (1999) argued that this

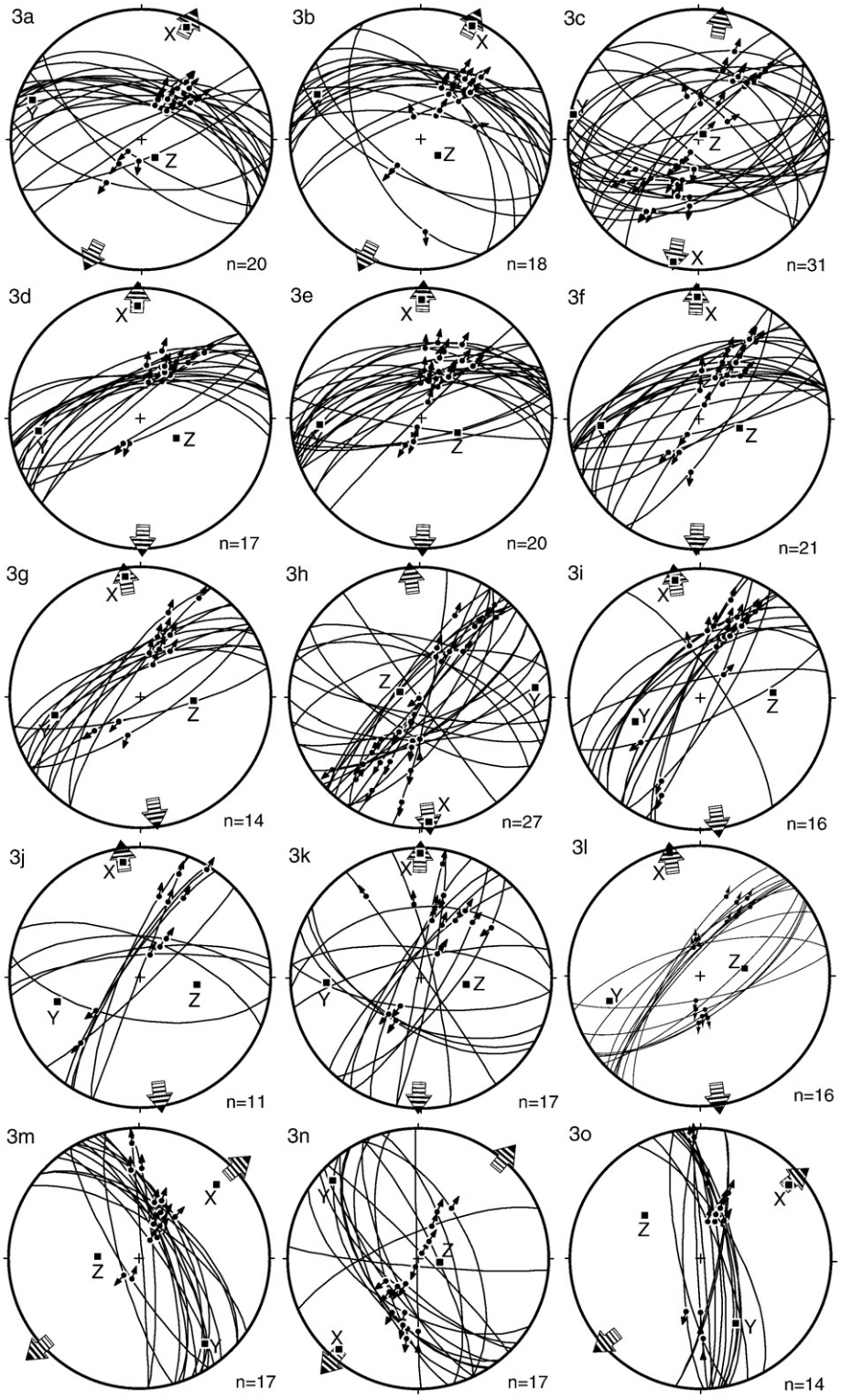

Fig. 5. Fault-slip data from western Turkey. (a–o) Youngest faulting increment; diagrams show great circle of fault plane and projected trace of slickenside lineation in lower-hemisphere equal-area projection; principal strain axes (X > Y > Z) shown, deduced extension directions (X) are indicated by hatched diverging arrows and shortening directions (Z) by black converging arrows; outcrop number shown on upper left and located in Fig. 4. (p–u) Older faulting increment characterized by E–W shortening and N–S extension.

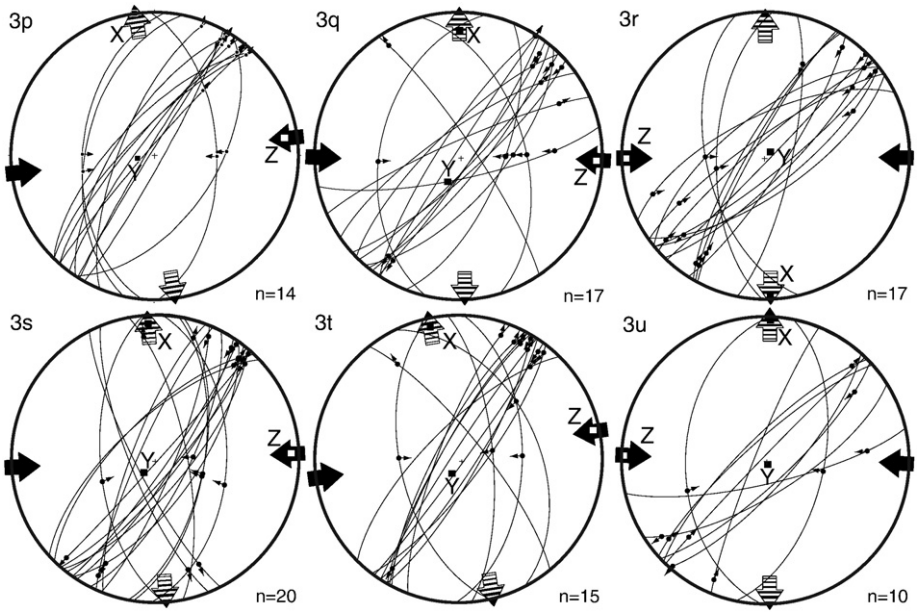

Fig. 5 (*continued*).

phase of extensional faulting occurred in a sinistral wrench corridor accommodating differential extension between the Aegean and western Turkey.

5.3. Ikaria Island

The extension history of Ikaria is relatively simple and characterized by low- and high-angle normal faulting from ~15–3 Ma (Kumerics et al., 2005; Beaudoin et al., 2015). The topography and the fault pattern on Ikaria Island is much simpler and distinctly different from that of the neighbouring islands of Samos and Fourni (Fig. 4). There is a set of mutually crosscutting E–W-striking normal faults and mainly NNE-striking, but also NW-striking strike-slip faults. Fault-slip data indicate that this fault set is due to NNE-directed extension (Fig. 7a–g). The NNE-striking faults are basically tear faults that accommodate heterogeneous extension on the normal faults.

Kumerics et al. (2005) and Beaudoin et al. (2015) showed that ductile extensional deformation commenced by ~15 Ma and that the high-angle normal faults are associated with ductile shear zones and cut them. Apatite (U-Th)/He data indicate that extensional deformation continued to be active at least until ~3 Ma (Kumerics et al., 2005).

The relatively simple style of extensional faulting on Ikaria Island is similar to that in the central Menderes Massif. The only exception being the timing as on Ikaria NNE-directed extension is seemingly ongoing since ~15 to 3 Ma, whereas in western Turkey extension at 24–19 Ma was followed by plateau formation and then renewed extension associated with the Central Menderes metamorphic core complex from ~5 Ma to the recent. A major difference is that there is no indication for a phase of E–W shortening interrupting or accompanying NNE extension on Ikaria Island.

5.4. Patmos Island

The geology of Patmos is dominated by late Miocene and Pliocene volcanic rocks. Wyers and Barton (1986) showed that the volcanics were derived from an upper mantle source, which contained a substantial component from the subducting slab and also an enriched alkaline within-plate component. The volcanics are grouped into an older main volcanic series with ages of 7–5.5 Ma and a young volcanic sequence with ages of 4.5–3.5 Ma (Wyers, 1987). There is also an undated older volcanic series. Wyers and Barton (1986) discussed that a tear-related asthenosphere source became important for Patmos lavas after ~7 Ma.

The faults on Patmos can be grouped into a young set that is closely related to the topography of the island and older faults that are crosscut by the young fault generation (Fig. 4). The major young faults either strike NW or E–W. Small-scale faults associated with the major faults displays heterogeneous data sets, either simple conjugated E–W-striking oblique normal faults (Fig. 8a) or NW-striking oblique normal faults (Fig. 8b). Most stations record a more varied set of faults (Fig. 8c–f). The derived extension direction is predominantly N–S, but E–W extension is also recorded locally (Fig. 8d).

The older faults strike preferentially N and do not affect the rocks of the young volcanic series and thus must be older than 4.5 Ma. Fault-slip data sets either show reverse faulting on N-striking faults (Fig. 8g) or, more commonly a more heterogeneous set of oblique-slip and strike-slip faults (Fig. 9h–k). Other stations show E–W-striking small-scale strike-slip faults (Fig. 8k, l). Despite the heterogeneity of the data sets, they all show subhorizontal shortening axes, which cluster around the E–W direction (Fig. 8g–k).

For Patmos, young extension is mainly N–S directed and overprinted a phase of E–W shortening between >7 and 4.5 Ma. This shortening phase was associated with the tear-related asthenosphere source affecting Patmos after ~7 Ma (Wyers and Barton, 1986). We did not find any evidence for an older faulting increment in the undated older volcanic series.

5.5. Amorgos Island

Amorgos experienced low-angle normal faulting at ~19–15 Ma (Rosenbaum et al., 2007; Ring et al., 2009), followed by folding about N–S axes resulting from WNW–ESE shortening and subsequent high-angle normal faulting (Rosenbaum and Ring, 2007). The normal faults offshore Amorgos became famous in 1956 when the two largest recent earthquakes in the south Aegean region occurred within only 13 min from each other and had magnitudes of 7.4 and 7.2 (Papadopoulos and Pavlides, 1992). Both events were located between Santorini and Amorgos (Dimitriadis et al., 2009). Focal-plane solutions and neotectonic analysis shows NW–SE oriented extension associated with the earthquakes (Papadopoulos and Pavlides, 1992; Papazachos et al., 2000). The northwest coast of the island subsided whereas the southeast coast was uplifted (Stiros et al., 1994) indicating rotation about a

horizontal axis in the footwall of a SE-dipping normal fault. Dimitriadis et al. (2009) investigated the active tectonics of the Coloumbo volcanic center along the Amorgos-Santorini fault zone and most of their focal-plane solutions show NW extension as well (some events show N–S extension). Friedrich et al. (2014) also derived NW extension (155°/12°) from focal mechanisms.

There are a number of major NE-striking faults that control the topography of Amorgos and crosscut all other faults (Fig. 9). Fault-slip analysis supplies rather simple fault sets with either conjugate NE-striking faults (Fig. 10a–f) or single sets (Fig. 10g–l). There is one single location that yielded a set of NE-striking sinistral and dextral strike-slip faults (Fig. 10m). All locations provide a very consistent NW extension

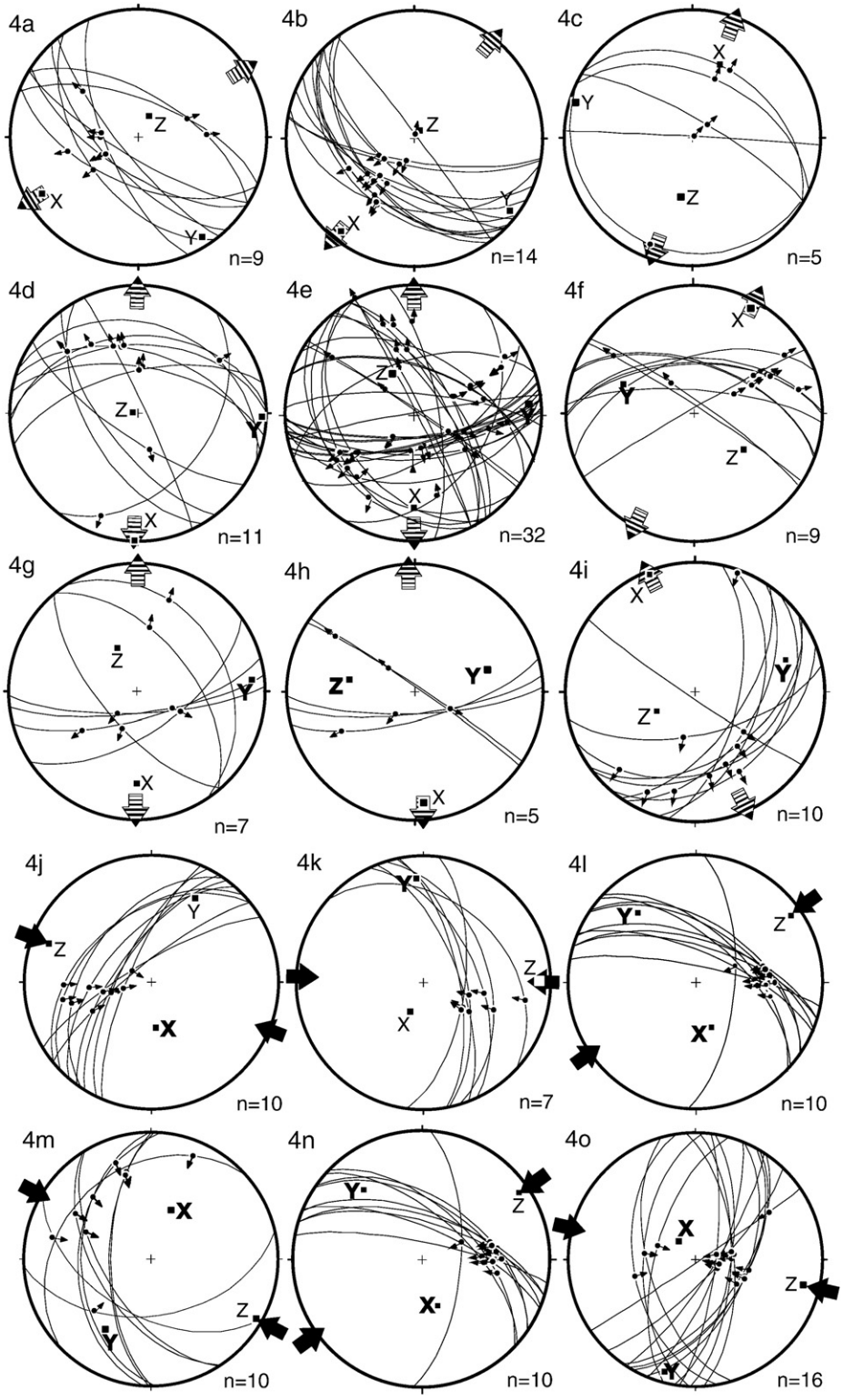

Fig. 6. Fault-slip data from Samos and Fourni islands; subdivision into increments of faulting principally based on crosscutting faults. (a–i) Youngest faulting increment characterized by N- to NE-directed extension. (j–p) Second youngest increment showing NE- to ESE-directed shortening. (q–u) Oldest increment characterized by E–W but also N–S extension.

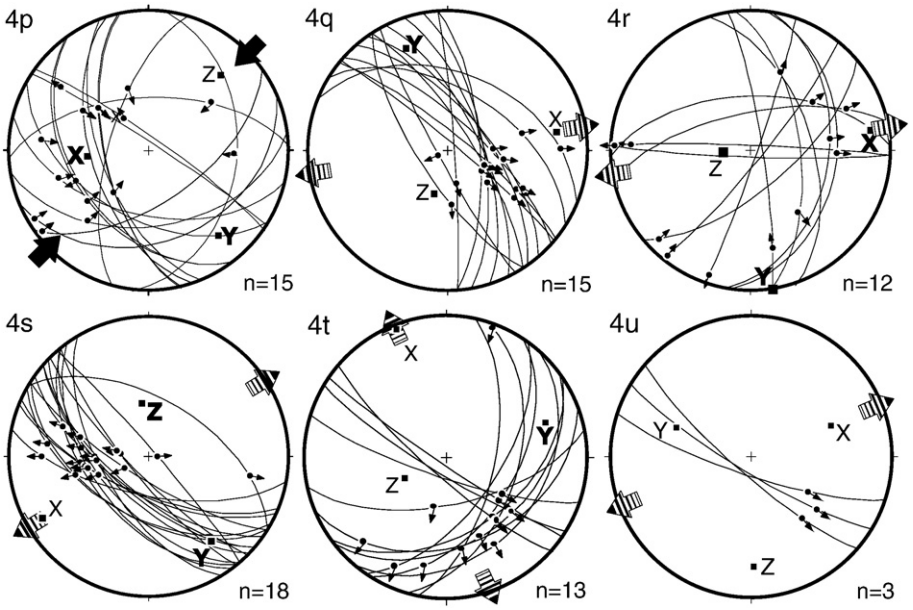

Fig. 6 (*continued*).

direction. There are a number of E–W-striking faults that are, in part, crosscut by the major NE-striking faults (Fig. 9). Fault-slip analysis from these faults shows N–S to NNW extension (Fig. 10n–u). Furthermore, there is an older set of NE-striking faults with conjugate (Fig. 10v) and W-dipping (Fig. 10w) reverse faults. These faults sets provide WNW-directed shortening axes.

There are hardly any age constraints for the various fault generations on Amorgos. The youngest set of NE-striking faults is still active but it is

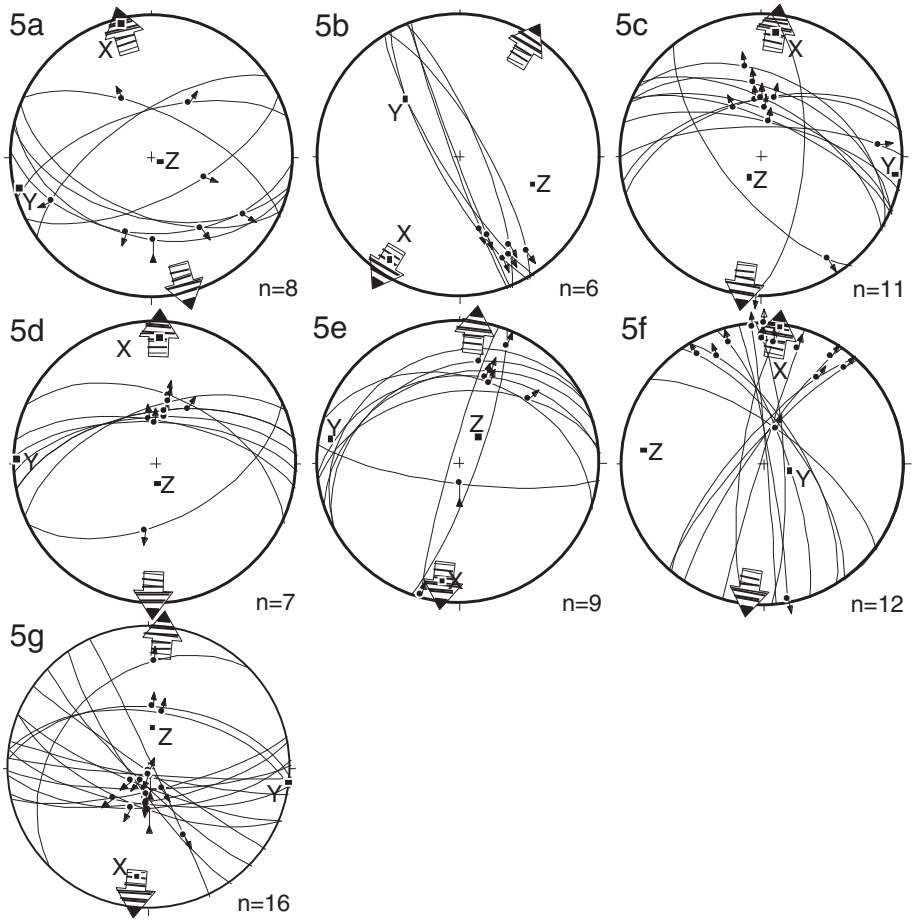

Fig. 7. Fault-slip data from Ikaria Island showing relatively simple pattern of faults resulting from N- to NNE-directed extension.

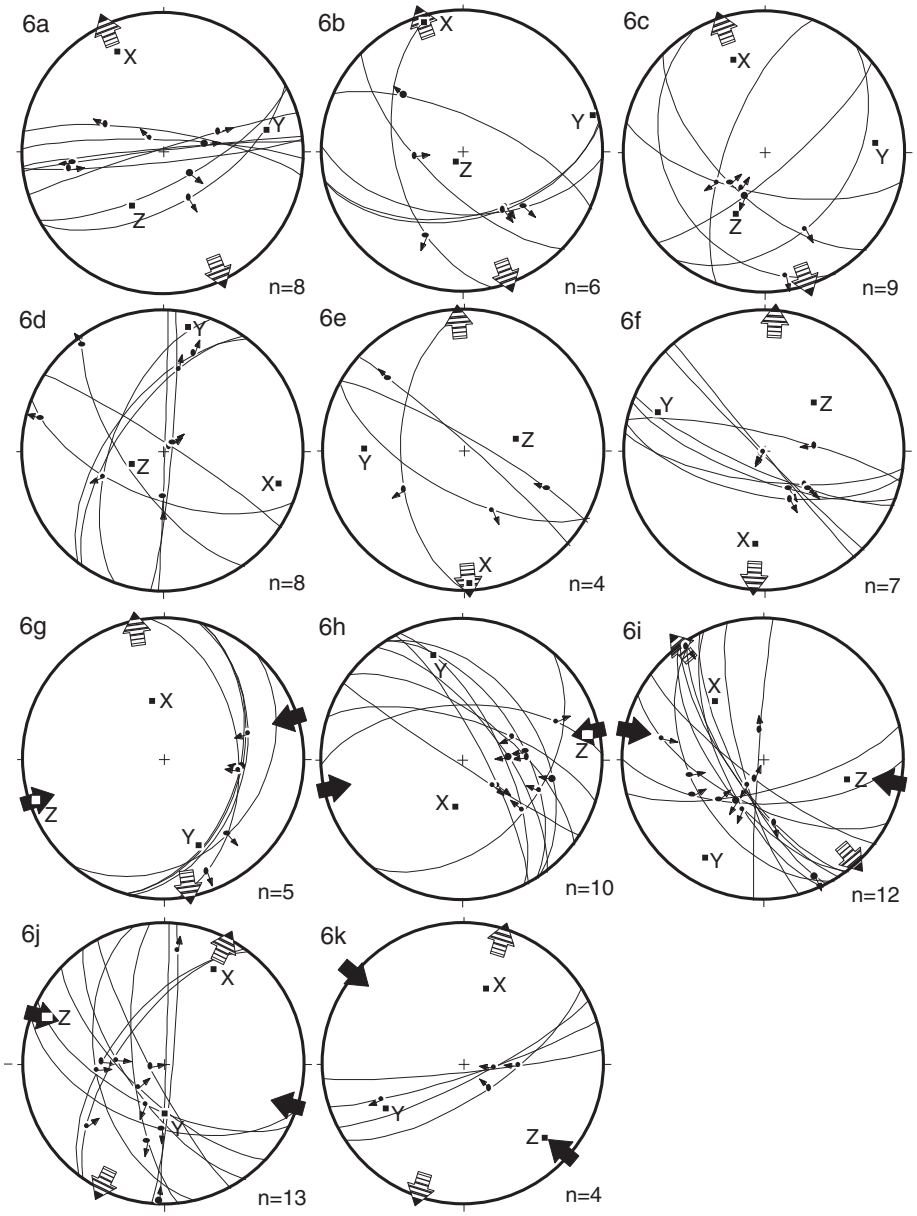

Fig. 8. Kinematic data from Patmos Island. (a–f) Youngest set of faults providing N–S-directed extension. (g–k) Older fault set showing E–W-directed shortening.

unknown when N- to NW-directed extension commenced. Likewise, the age of WNW–ESE shortening is not known. Ring et al. (2009) reported apatite fission-track ages ranging from 25.4 to 15.2 Ma. Based on these ages Chatzaras et al. (2011) placed WNW–ESE shortening into the mid Miocene (~16–11 Ma). However, the shortening event can also be younger than mid Miocene.

5.6. Astipalia Island

The faults on Astipalia can be grouped into three generations (Ring, 2001). There are two sets of E–W-striking faults, and the younger of these sets crosscuts NE-striking faults (Fig. 9). There are four major young E–W-striking faults in the north and fault-slip data indicate N–S extension associated with these faults (Fig. 11a–c). The next older fault generation is a set of NE-striking faults. Fault-slip analysis shows that this set can be subdivided into reverse faults, sinistral and dextral strike-slip faults, and a few normal faults (Fig. 11d–h). All data show WNW-directed shortening with subvertical to moderately plunging extension axes. The oldest set of faults provides a fairly simple pattern of mainly NW-dipping normal faults (Fig. 11i–l) that resulted from NW-directed extension.

Despite consistent crosscutting relations of fault generations there is basically no absolute age control on the faults on Astipalia Island. Faulting must be younger than Paleocene to Eocene marls, which are cut by all three faults sets (Ring, 2001).

5.7. Eastern Crete

Crete has undergone extension since the mid Miocene. Extension was first by N–S directed low-angle faulting along the Cretan detachment (Fassoulas et al., 1994) and associated upper crustal N–S extension along high-angle faults forming graben in Crete by ~12–10 Ma (Fassoulas, 2001; Ring et al., 2001; Seidel et al., 2007). N–S extension was followed by a period of E–W extension after ~10 Ma (van Hinsbergen and Meulenkamp, 2006). The recent kinematic regime started during the Pliocene, and is largely characterized by N–S

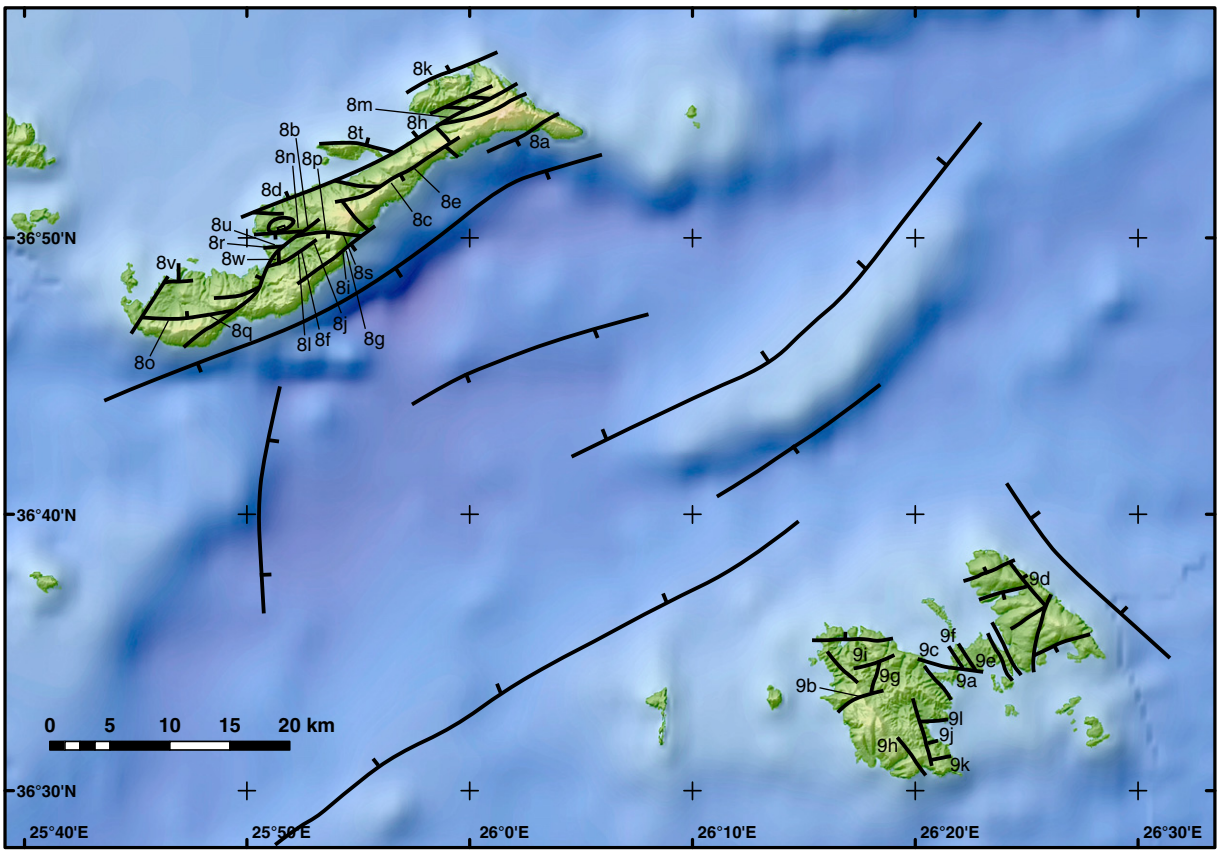

Fig. 9. Topographic map of Amorgos-Astipalaia with major onshore and offshore faults and locations where fault-slip data were collected; map modified from Ring (2001), Bohnhoff et al. (2006), Rosenbaum et al. (2007), Rosenbaum and Ring (2007).

extension in central Crete and a component of radial to E–W extension in western and eastern Crete (Angelier et al., 1982; Ring et al., 2001, 2003b; Caputo et al., 2010; Gallen et al., 2014).

We mapped kinematic data on a set of faults in east Crete (Fig. 12). The major faults strike NNE and control the topography. These young faults cut older E–W-striking faults (Fig. 12). The youngest set of NNE-striking faults provides an E–W to WNW–ESE extension direction (Fig. 13a–i). Fault slip data from the older set of faults indicates mainly N–S extension (Fig. 13j–s). In almost all cases the shortening directions are subvertical, indicating normal faulting.

Our results are in agreement with earlier work by Angelier et al. (1982) and Fassoulas (2001), arguing that the Pliocene to Recent extension direction in east Crete is E to ESE. In central Crete the neotectonic extension direction is mainly N–S, but local E–W extension is also observed (Angelier et al., 1982; Fassoulas, 2001; Ring et al., 2003b; Caputo et al., 2010; Gallen et al., 2014).

6. Tectonic interpretation

We interpret the data sequentially from young to old events using mainly our data but also published data. The grouping into age brackets is, in part, somewhat arbitrary and has been done to facilitate the discussion. The presented fault-slip data are complex and regionally variable. In general, they show horizontal extension, dominantly in the NNE direction. In western Anatolia, Samos, Patmos, Amorgos and Astipalia the data show a phase of E–W shortening, which is not always well constrained chronologically.

6.1. Youngest extension

The youngest data set is characterized by horizontal extension in various directions (Fig. 14a). The extension direction is largely NNE oriented in the central and northern Aegean and a mix of NNE oriented and radial extension from about south of latitude 37°S. The fault-slip data agree with earthquake focal-plane solutions and the strain-rate directions as derived from the recent velocity field (Kahle et al., 1999; Papazachos et al., 2000; McClusky et al., 2000).

The young extension phase might be explained by local arc-parallel extension in the southern Aegean superposed on regional NNE extension driven by slab retreat. The directions and magnitudes of the GPS-derived velocities depicted in Fig. 1b shows that the current velocity field is controlled by the SSW-ward retreat of the Hellenic slab. Most workers conclude that Hellenic slab retreat has controlled NNE oriented extension in the Aegean Sea region since the early Miocene (see reviews by Jolivet and Brun, 2010; Ring et al., 2010). In the southern Aegean, Africa-Europe convergence at rates of ~8 mm/a exerts a N–S shortening component (Kahle et al., 1999), which together with slab retreat and the increasing curvature of the Hellenic arc would result in a flattening strain field characterized by variable extension directions in the southern half of the map shown in Fig. 14a. The extending Aegean crust has pre-existing anisotropies, which may add to influence local extension directions.

The directions obtained from the fault-slip data shown in Fig. 14a represent time-averaged extension directions over a few million years. It is hardly known when this extension phase deduced from the fault-slip data started and it may have commenced at different times in different regions. In western Anatolia, E–W striking normal faults are the young, seismically active, uppermost crustal expression of the bivergent detachment fault system of the Central Menderes core complex that started operating by ~5 Ma (Gessner et al., 2001; Ring et al., 2003a). Zircon (U-Th)/He ages of ~4–2 Ma (Buscher et al., 2013) and apatite-fission track ages as young as ~1.6 Ma suggest that high-angle normal faulting commenced by about ~4–2 Ma. Buscher et al. (2013) have shown that this cooling phase was primarily controlled by normal

faulting and that erosion was a minor cooling/exhumation agent. A similar scenario applies to the data set from Ikaria Island, where the extension direction of brittle normal faulting is co-directional with the extension direction of earlier low-angle detachment faulting (Kumerics et al., 2005; Beaudoin et al., 2015). Apatite (U-Th)/He data suggest that high-angle normal faulting commenced after ~3 Ma (Kumerics et al., 2005). In Crete, the latest phase of extensional faulting started in the Pliocene (~5 Ma) (Angelier et al., 1982; Caputo et al., 2010), an age that is similar to the onset of N–S extension on Patmos (~4.5 Ma). On Samos, high-angle normal faulting due to NNE extension commenced earlier at 8.6 Ma (Ring et al., 1999).

This summary of available age constraints highlights the importance of the ~5–3 Ma time window for the onset of the young stage of extension, except for Samos at the Aegea-Anatolia boundary zone where this extension phase started earlier. At ~5–3 Ma a number of important tectonic changes occurred along the wider Aegea-Anatolia plate boundary: (1) The North Anatolian Fault propagated into the northern Aegean Sea region (Barka, 1992; Şengör et al., 2008); (2) the second phase of extension and core complex formation commenced in the central Menderes Massif (Gessner et al., 2001, 2013; Ring et al., 2003a), segmenting a continuous plateau in the footwall of the earlier stage core-complex formation; (3) the Libyan continental margin started to collide with Aegea (Kopf et al., 2003).

6.2. Intermittent E–W shortening

The more challenging data to interpret are those showing E–W shortening as seen in west Turkey, Samos/Fourni, Patmos, Amorgos and Astipalaia. Late-stage brittle E–W shortening has also been reported by Menant et al. (2013) from Mykonos Island. Large-wavelength, low-amplitude folding with axes subparallel to the extension direction resulting in prolate strain have been described by Avigad et al. (2001) from Andros, Naxos and Paros, and by Gessner et al. (2013, 2016) from the northern Menderes Massif (Fig. 14b).

The best age constraints are from Samos Island, where crosscutting relations in dated sediments show that E–W shortening was a short-

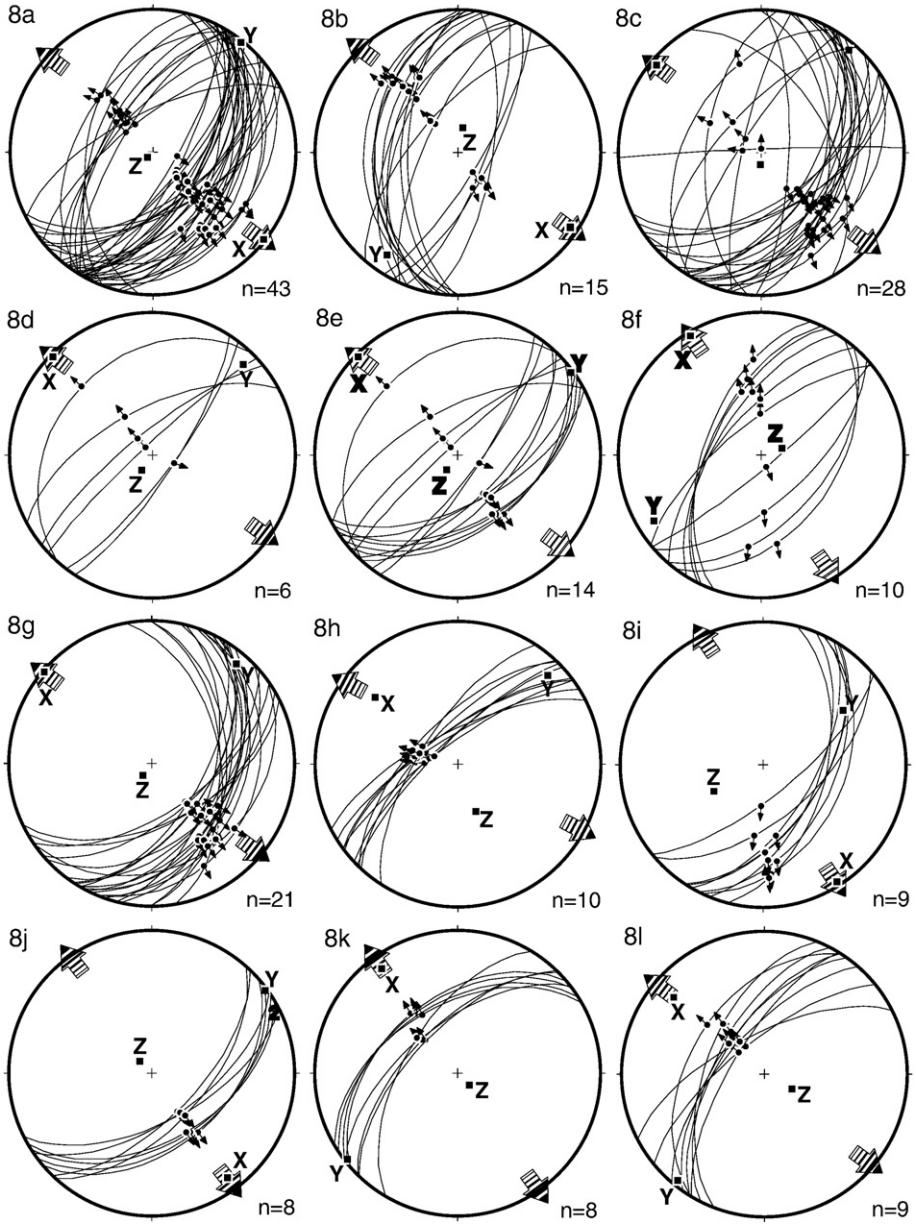

Fig. 10. Fault-slip data from Amorgos Island. (a–u) Young increment shows consistent data sets resulting from NW- to NNW-directed extension. (v–w) Older increment resulting from ESE-directed shortening.

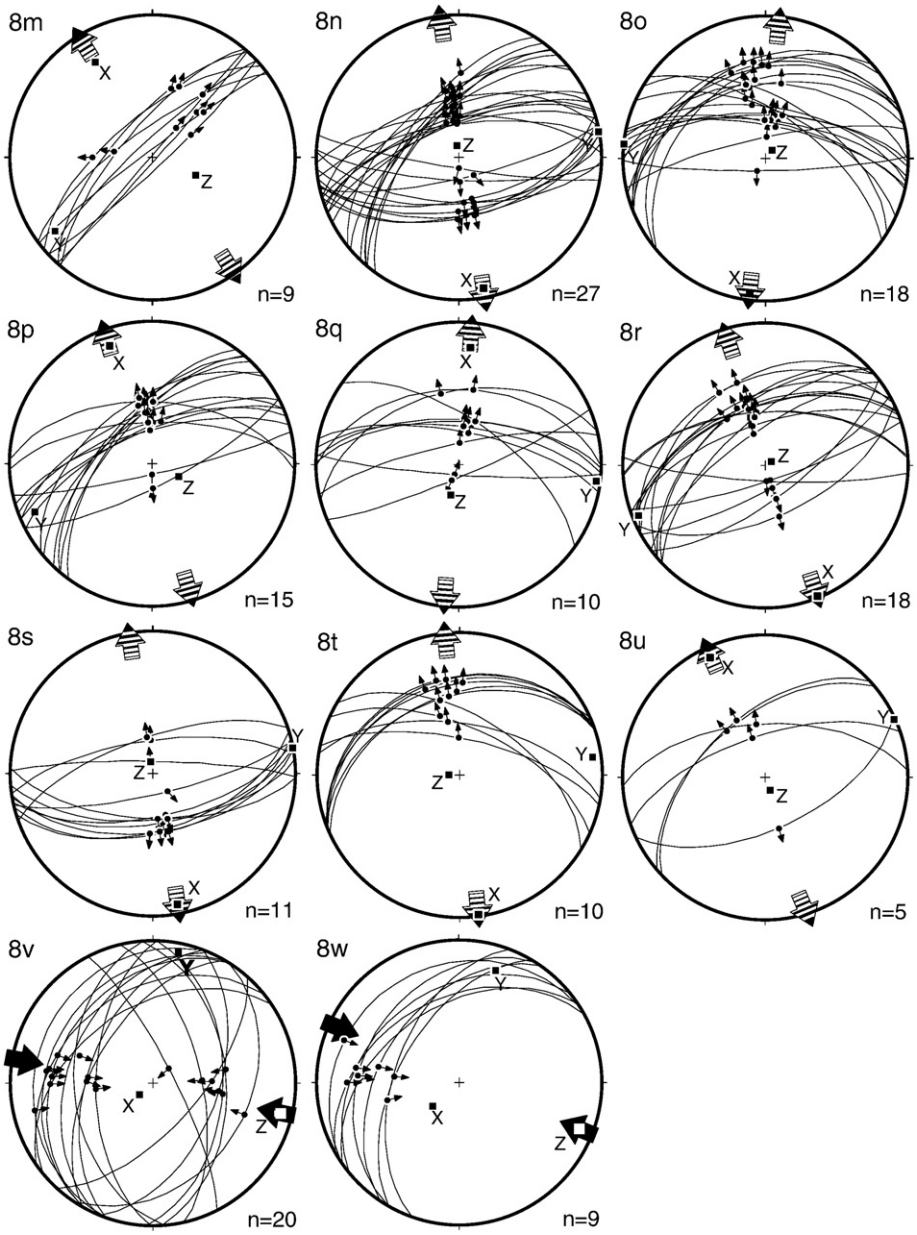

Fig. 10 (*continued*).

lived event at 9–8.6 Ma (Ring et al., 1999). Menant et al. (2013) speculated that E–W shortening on Mykonos would fit into this time frame. On Patmos, shortening occurred later at >7–4.5 Ma, whereas along the west Turkish coast it is less well constrained in time and occurred between ~12–5 Ma. Sümer et al. (2013) suggested that E–W shortening occurred at ~5 Ma. We propose that this deformation phase was finished by ~5 Ma as the prominent low-angle detachments in the central Menderes Massif are not deformed by E–W shortening. All the so far discussed shortening structures are completely brittle.

There are also shortening structures that started to form in the ductile crust and continued to be active after the rocks passed the brittle-ductile transition during exhumation. Grasemann et al. (2012) and Rabillard et al. (2015) described ductile-to-brittle shortening normal to the extension direction associated with late Miocene pluton emplacement in the western Aegean. The folds reported by Avigad et al. (2001) from Paros and Naxos in the central Aegean also formed during extensional deformation, folded the brittle Naxos/Paros detachment surface and affected the syn-extensional migmatite and granodiorite in the footwall of the detachment. The concentric pattern of mineral isograds around the Naxos migmatite dome (Jansen and Schuiling, 1976) is distinctly less intensely folded than the schist/marble sequence in which the isograds formed (Linnros, 2016). The isograds probably formed at the peak of high-grade metamorphism at ~16–14 Ma (Wijbrans and McDougall, 1988; Martin et al., 2006; Bolhar et al., 2017). The Naxos granodiorite intruded at 13–12 Ma into an antiform related to late-stage folding. Collectively this suggests that the folds started to form >16–14 Ma. This together with low-temperature thermochronology data (Brichau et al., 2006; Seward et al., 2009) places E–W shortening to between >16–14 and 8 Ma on Naxos/Paros. In the footwall of the Simav detachment in the northern Menderes Massif, E–W shortening was coeval with ductile extension and emplacement of the Egrigoez pluton between 24 and 19 Ma (Gessner et al., 2013). These timing constraints show that E–W shortening was not a single deformation phase that that affected the various study areas simultaneously.

In general, the amount of E–W shortening is modest. Cross sections by Ring et al. (1999) show that shortening on Samos is <10%. For Naxos, Linnros (2016) quantified shortening in various balanced E–W profiles and showed that shortening is highest in the migmatite dome

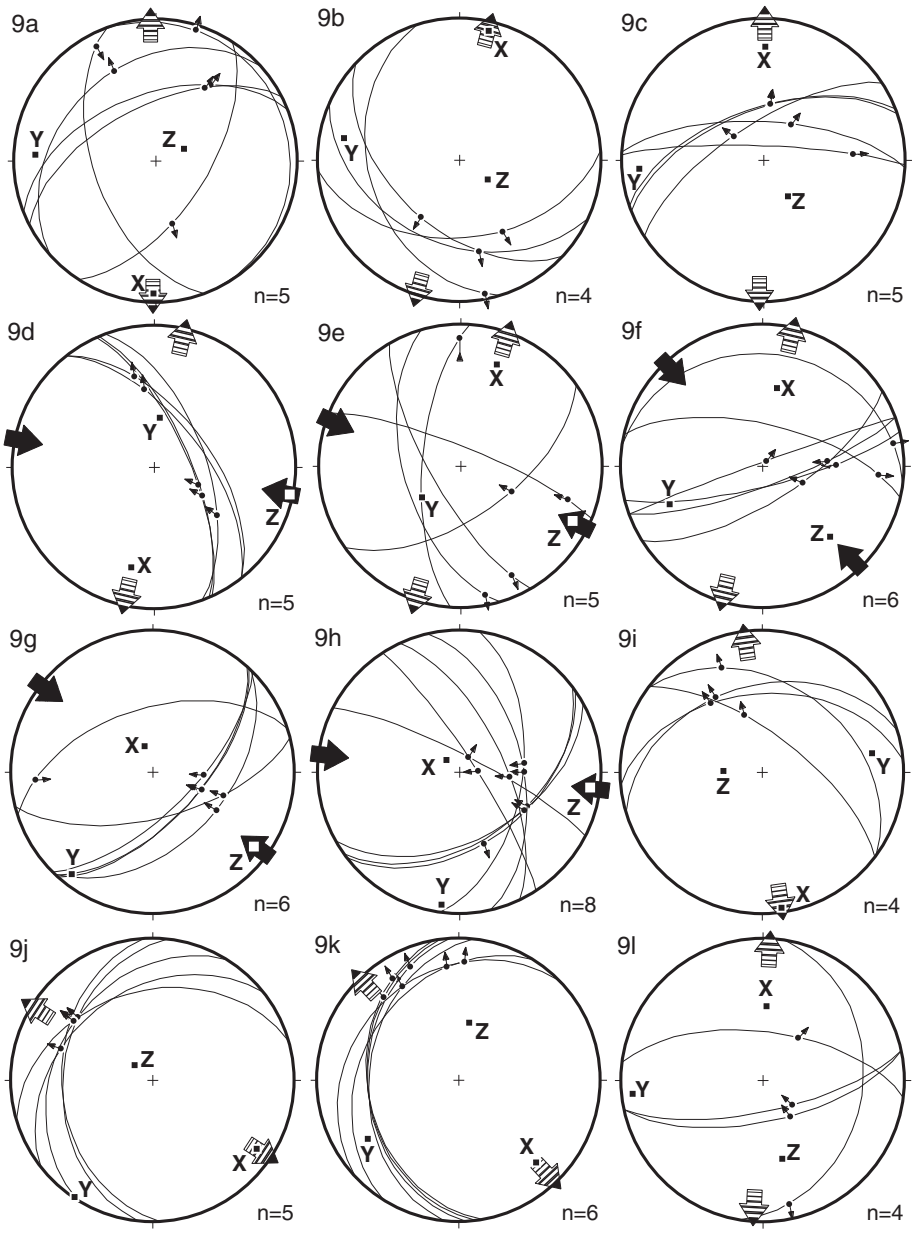

Fig. 11. Kinematic data from Astipalaia Island. (a–c) Youngest increment showing N–S extension. (d–h) Second youngest increment providing E- to SE-directed shortening. (i–l) Oldest data set showing NW- to N-directed extension.

(minimum of 15–18%) and becomes less N and S of the dome (minimum < 7%). The migmatite on Naxos is a result of extensional deformation (Buick and Holland, 1989; Martin et al., 2006). The relation between extension-related metamorphic grade and amount of shortening on Naxos shows that E–W shortening is intimately associated with N–S extension, the latter of which lasted from >20 Ma until ~8 Ma (Brichau et al., 2006).

E–W shortening was, at least in part, coeval with N–S extension and broadly occurred between 16 and 5 Ma (the northern Menderes Massif would be an exception). The Cyclades in the central Aegean experienced a surge of extensional deformation at ~15–8 Ma characterized by abundant fission-track cooling ages in the footwalls of major extensional faults and intrusion of I-type plutons (see summary in Ring et al., 2010; Bolhar et al., 2010; Bargnesi et al., 2012) (Fig. 3). These coincidences in the timing suggest that there is a causal relationship between large-scale extension, pluton emplacement and E–W shortening.

What caused E–W shortening during N–S extension in the Aegean and west Turkey? Laws et al. (1997) and Menant et al. (2013) speculated that shortening is due to the westward escape of Anatolia in the late Miocene. E–W shortening is not a single event and occurred variably in time. However, most workers regard the westward escape of Anatolia as a rather continuous event, which, if responsible for E–W shortening in the eastern Aegean, should have affected the rocks on the various islands in a rather systematic fashion in space and time. Furthermore, Anatolian escape occurred too late to explain shortening starting at 16 Ma and earlier.

E–W shortening may in part reflect local adjustments to increasing curvature of the Hellenic arc that may have happened systematically along the margins of the highly extended Aegean region (i.e. Samos, Paros, Amorgos, Astipalia, Turkish coast in the E, but also Lavrion, Evia, Peleponnesos in the W). In the east, E–W shortening appears to be a local deformation phase apparently not always coeval with N–S

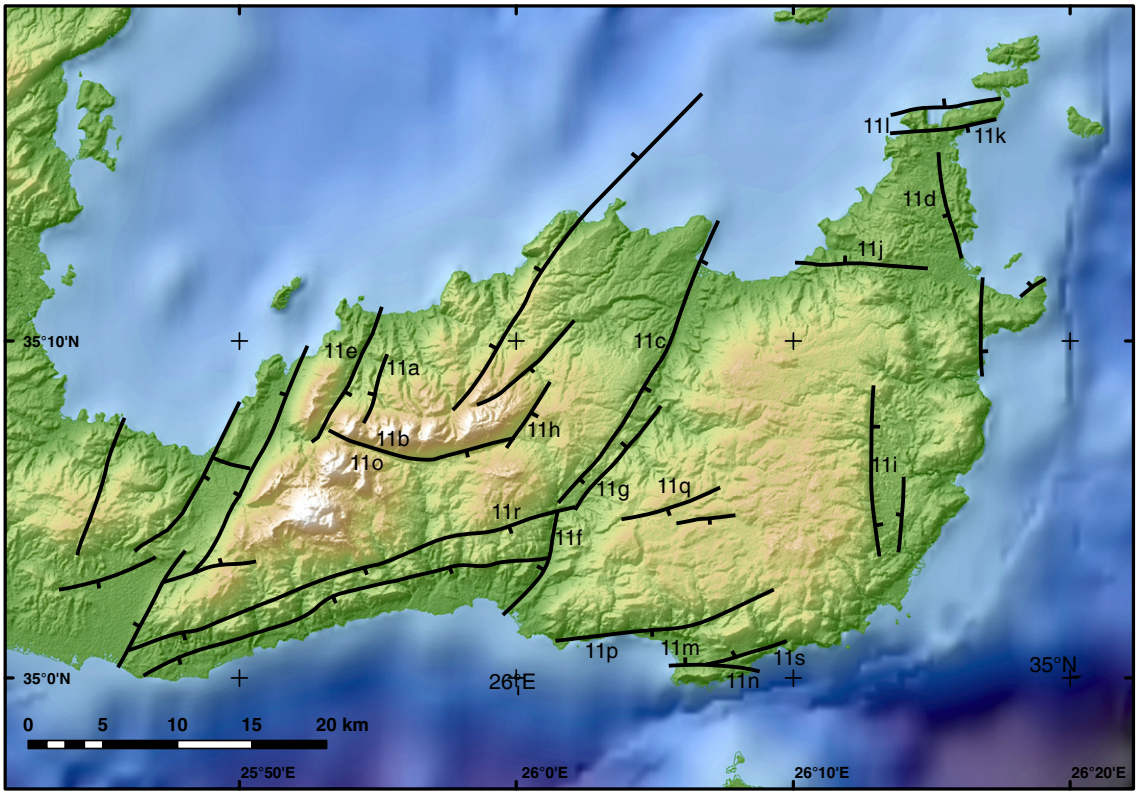

Fig. 12. Topographic map of east Crete with major faults and locations where fault-slip data were collected; fault pattern modified from Creutzburg et al. (1977).

extension. If so, the cause for E–W shortening might not be the same for all study areas. If E–W shortening is curvature controlled, then similar structures should occur in the west but have not been reported from Evia (Ring et al., 2007b), Lavrion (Berger et al., 2013) and the Mani peninsula of the eastern Peleponnesos (Micheuz et al., 2015). However, E–W shortening structures do occur at least in some western Aegean Islands (Grasemann et al., 2012; Rabillard et al., 2015). We tentatively suggest that the increased curvature of the Hellenic arc was not important for local and intermittent E–W shortening. However, there appears to be a spatial association with brittle E–W shortening and the slab tear along the Aegea-Anatolia plate boundary (see below).

For answering what caused E–W shortening it might be important to distinguish between the large-wavelength folding in the central Cyclades and the northern Menderes Massif and upper crustal brittle reverse faulting near the Aegea-Anatolia plate boundary. Most of the total extension in the Menderes Massif occurred at 24–19 Ma and was resolved at the Simav detachment (Seyitoğlu et al., 2004; Thomson and Ring, 2006; van Hinsbergen, 2010; Ring et al., in preparation) (Fig. 2). The large-wavelength folding about NNE–SSW axes in the northern Menderes Massif formed in the footwall of the Simav detachment. Purvis and Robertson (2004, 2005) and Cemen et al. (2006) showed that in western Anatolia mid Miocene sediments commonly show onlap relations towards folded orthogneiss leading Gessner et al. (2013) to argue that large-wavelength folding due to E–W shortening was involved in controlling basin topography. Scaled physical experiments suggest that folding parallel to the extension direction is an unstable deformation mode, where elastic folding of the thin, elastic upper crust gets imposed on viscous mid- to lower-crustal layers (Venkat-Ramani and Tikoff, 2002; Lévy and Jaupart, 2011). Lévy and Jaupart (2011) argue that shortening is an elastic response perpendicular to extension without the need of externally imposed far-field shortening. The latter view is an elegant solution explaining large-wavelength folding coeval with large-scale extension as seen in west Turkey but also in Andros, Naxos and Paros (Avigad et al., 2001) and might well explain extension-parallel folding. This process seems to be restricted to regions with a highly ductile lower crust and a shallow brittle-ductile transition (Lévy and Jaupart, 2011). It can be speculated that the overall 3D crustal strain pattern represents a 'mode 3' partitioning of crustal strain sensu Axen et al. (1998), where different layers of the Earth's crust deform by different deformation mechanisms. The concept of dismembered upper crustal rafts floating on a spreading lower crust has shown to be consistent with stage 2 metamorphic core complex formation in the Menderes Massif by both numerical (Wijns et al., 2005) and geodetic inversion studies (Aktug et al., 2009). It can be speculated that the combination of SSW-directed slab rollback and the E–W gradient in gravitational potential that Özeren and Holt (2010) have identified as driving crustal extension in western Anatolia are reflected in this strain partitioning. Another similarity between large-wavelength folding in the central and western Aegean and the northern Menderes Massif is the intrusion of huge granodiorite bodies into folding-related antiforms associated with large-scale extension. In both regions, the central Cyclades (Serfios-Naxos-Paros-Mykonos-Andros) and the northern Menderes Massif, large-wavelength folding occurred when the regions experienced a large amount of N–S ductile extension. If accepted, this view would explain why the timing of large-wavelength folding is different in those two regions.

The much smaller wavelength distinctly brittle structures seen in western Anatolia and the east Aegean Islands cannot be explained in the same way as the large-wavelength folding. The middle and lower crust in this region close to the Aegea-Anatolia plate boundary broadly coincides with a cluster of older fission-track ages. This phase of brittle E–W shortening is not associated with large-scale extension. The timing constraints from Samos and Patmos appear to show some overlap with alkaline magmatic activity on those two islands at 11–8 Ma (Samos, Pe-Piper and Piper, 2007) and ~7 Ma (Wyers and Barton, 1987). At the least, the regional variation in the orientation of brittle structures

suggests lateral mechanical decoupling between western Anatolia and the central Aegean Sea region along this corridor.

6.3. Older extensional phase

Since the early Miocene (~24–23 Ma) and before ~19 Ma, the Cyclades and west Turkey underwent wholesale NNE extension driven by slab retreat (Jolivet and Brun, 2010; Ring et al., 2010; Grasemann et al., 2012; Gessner et al., 2013). Samos Island represents an exception in this general picture because extension on Samos was E–W directed between ~20–14 Ma (Ring et al., 1999; Kumerics et al., 2005; Gessner et al., 2011). The oldest increments of the fault-slip data on Samos also show E–W extension (Fig. 6q–u), which are probably an upper-crustal expression of ductile E–W extension at ~20–14 Ma. Ring et al. (1999) explained the anomalous E–W extension direction to reflect formation of a sinistral wrench corridor accommodating differential extension between the Aegean and west Turkey. The extensional detachments in west Turkey taper out to the west while the Aegean detachments have not laterally propagated into west Anatolia (Fig. 14c). For instance, the North Cycladic detachment system propagated eastward and became active on Ikaria at ~15 Ma (Kumerics et al., 2005; Beaudoin et al., 2015) and at ~10 Ma on Samos (Kumerics et al., 2005). In map view, the geometry of the low-angle detachments in the Aegean Sea are separated from those in west Turkey, i.e. they are two spatially separated extension provinces. This separation is also indicated by the fission-track age maps in Fig. 3. The Aegean Sea region shows a sizable region of young ages (<14 Ma) and an associated surge in extensional deformation in the middle/late Miocene. This is not the case in the Menderes Massif, where only a small region of ages <5 Ma occurs. The different age patterns suggest that both regions are separated by a tectonic discontinuity, probably expressed as the apparent left-lateral offset in the Miocene fission-track ages between Aegea and west Anatolia.

Simple 3D elastic models of two simultaneously moving laterally tapering detachment fault systems should cause extension perpendicular to the slip directions between the two detachment systems (Bernhard Grasemann, written communication, 2011) and we propose that E–W extension on Samos Island accommodates extension perpendicular to the main extension direction. The fission-track cooling ages suggest that E–W extension and the wrench corridor commenced in the early Miocene. The early Miocene Simav detachment had an offset of 50–90 km (Thomson and Ring, 2006; van Hinsbergen, 2010) and accommodated most of the total extension in the Menderes Massif. After movement on the Simav detachment ceased by 19 Ma (Thomson and Ring, 2006) no significant extensional structure operated and a mid-Miocene peneplain formed on the west Turkish plateau (Yilmaz et al., 2000). There is hardly any cooling recorded by fission-track ages at this time. This indicates highly differential extension between the Aegean and western Turkey since the early/mid Miocene (Gessner et al., 2013). Because the differentially extending regions were separated by a wrench corridor that, at least in part, was characterized by E–W extension, the major extensional detachment in the Aegean Sea region and the Menderes Massif are different structures that are not connected with each other.

Recent reviews on the role of slab tearing along the Aegea-Anatolia transition by Gessner et al. (2013) and Jolivet et al. (2015) proposed that progressive tearing commenced by about 20–16 Ma. Such a view is broadly in line with the onset of alkaline magmatism in west Turkey (~16–15 Ma according to Altunkaynak et al., 2010; 20 Ma according to

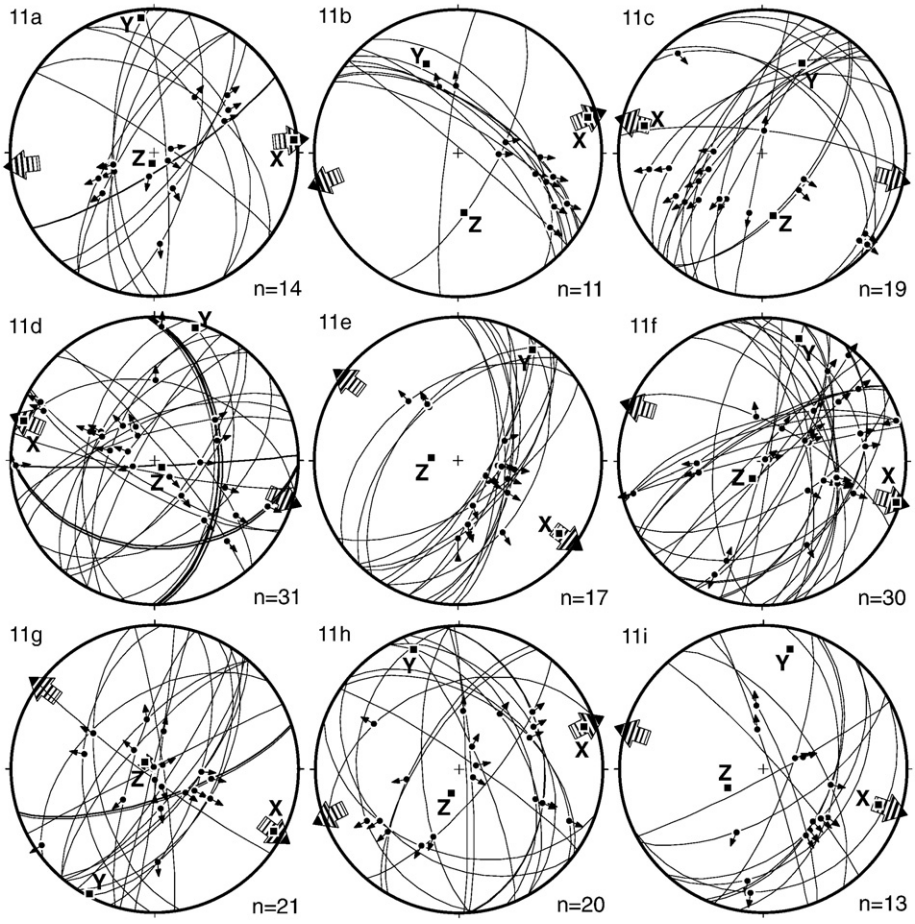

Fig. 13. Fault-slip data from east Crete. (a–i) Youngest increment characterized by E-W extension). (j–s) Older increment providing N–S oriented extension direction.

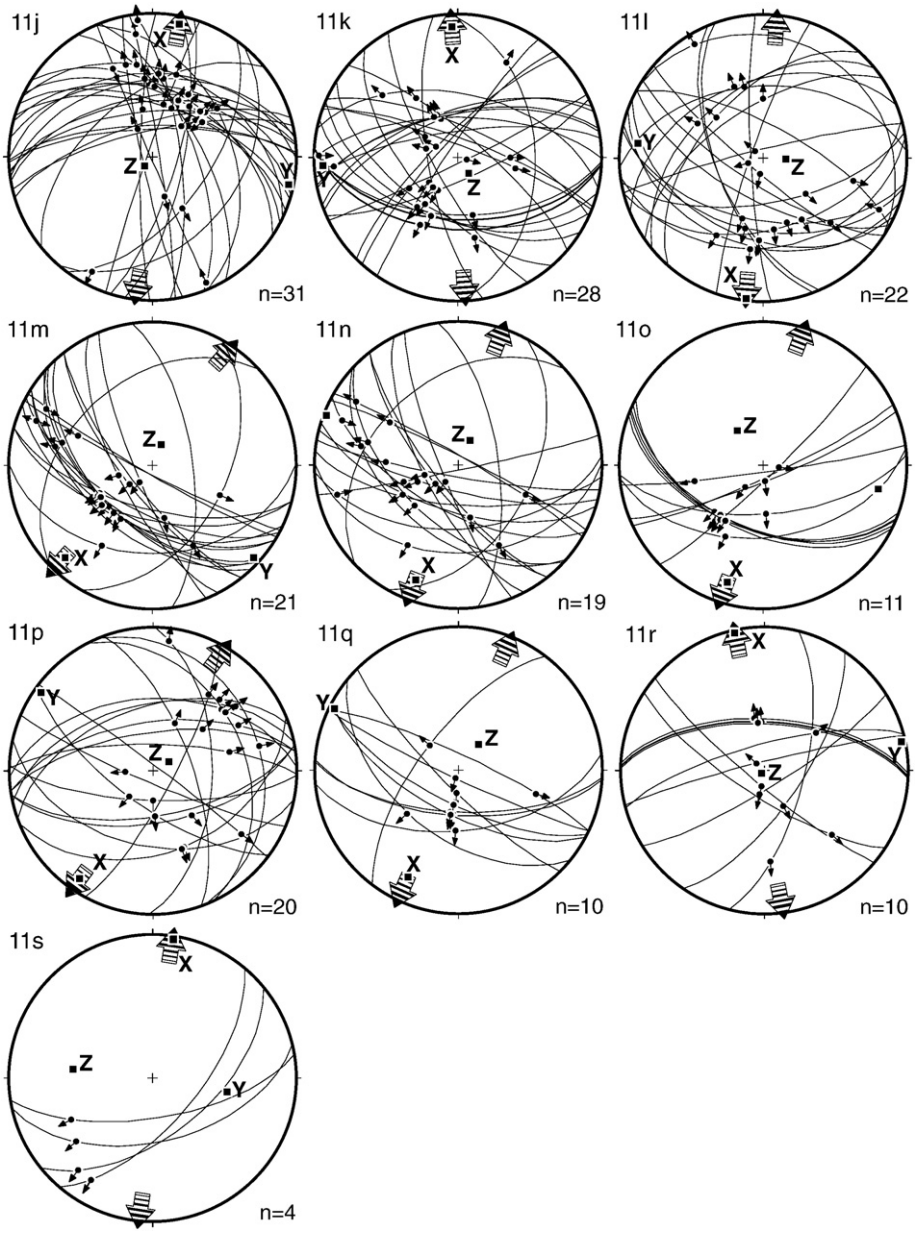

Fig. 13 (*continued*).

Prelevic et al., 2010). Prelevic et al. (2010) showed that alkaline magmatism between 20 and 4 Ma propagated from N to S. The formation of the mid Miocene plateau in the Menderes Massif is probably a consequence of the slab tear (see slab contours and slab window in Fig. 2). The diffuse Aegea-Anatolia plate boundary would have started to form in the early Miocene at the western edge of the northern Menderes Massif, expressed in the upper crust as a southward propagating structural corridor that accommodated differential extension. Given a response time of ~5 Ma, the structural expression of slab tearing should have occurred by 16–15 Ma on Samos Island and by 12 Ma on Patmos, but this proposition remains speculative.

6.4. Comparisons with focal-plane and GPS data

An interesting, but also challenging and speculative issue, is to assess how far the present-day GPS velocity field can be extrapolated back in time. To directly compare the recent velocity field shown in Fig. 1b with the extension directions derived from kinematic analysis, we plotted the extension directions calculated by Kahle et al. (1999) from the recent velocity field (Fig. 1c).

Our fault-slip data do not allow tight constraints to be put on the timing of the faulting increments. It might well be that those young increments that coincide directionally with focal-plane data and the GPS-derived directions represent the very youngest faulting phase and that increments with more varying directions are older (essentially Plio/Pleistocene) in age. In general, the match between extension directions from fault-slip data sets, strain rates calculated from the recent velocity field by Kahle et al. (1999) and Aktug et al. (2009), and those derived from earthquake focal solutions is good (Fig. 14a). There are some mismatches in the Paros-Naxos-Amorgos region. One reason for this might be that the fault-slip data reflect relatively old increments. However, this argument does not explain the almost 90° difference in extension directions between velocity-field-derived extensional strain rates and the extension directions from the 1956 Amorgos earthquakes. Overall, the recent velocity field can be tentatively extrapolated back into the Pliocene, as previously expressed by Le Pichon and Angelier (1981) and restated by Pérouse et al. (2012). Tectonic reorganisations at ~5–

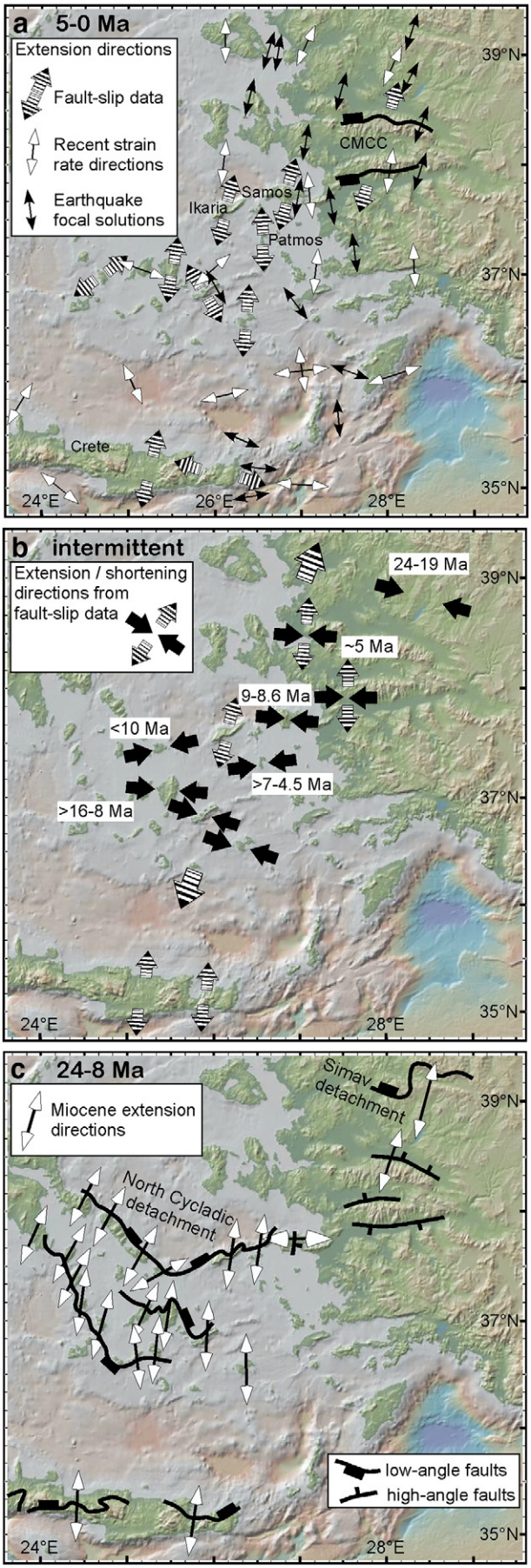

3 Ma thus appear to have resulted in the tectonic boundary conditions that have persisted until the recent.

For the older deformation increments possible matches between strain axes derived from fault-slip analysis and those from focal-plane and GPS data are less likely. Before ~5–3 Ma, extension was N to NE oriented, with the exception of the early/mid-Miocene E–W extension direction on Samos Island (Fig. 14b, c). Another potential mismatch between present day and Miocene extension directions are the arc-parallel extension directions seen in the present data. As discussed above, E–W extension on Samos can be explained by extension perpendicular to the slip directions between the two simultaneously moving laterally tapering detachments. However, an alternative scenario might be that E–W extension on Samos reflects a radial extension component controlled by initial Hellenic slab retreat and southward progressing slab tearing. Such a scenario would be similar to that presently seen in the southeast Aegean Sea (Fig. 1), highlighting that slab tearing propagated southward.

A possible match between the recent velocity field and the data showing E–W shortening depends on whether shortening is related to far-field shortening or not. In the last section we argued against upper crustal E–W shortening on the east Aegean Islands being caused by an elastic response to large-scale extension. Likewise, the recent shortening strain rates calculated by Kahle et al. (1999) appear to be too small to explain the ~10% shortening that accumulated over <0.5 Ma in Samos at 9–8.6 Ma.

Two scenarios might be envisaged: (1) The structures from which our data were collected had insignificant displacements that would not be captured by short-time GPS surveys and therefore our data have no implications on how far back in time the focal-plane and GPS data can be extrapolated. (2) We think it is much more plausible that the current GPS data do not record Aegean-Anatolia deformation before ~5–3 Ma and should not be interpolated beyond what they are: a snapshot of the recent velocity field. We believe that the Aegean-Anatolia upper crust deformed heterogeneously in time and space and the GPS data only track the very last stages of this deformation. Especially the strongly differential extension in the early/mid Miocene and the kinematics that resulted from this are not expressed by the focal-plane and GPS data. The interplay of varying extension directions and local and punctuated shortening deformation largely reflects local adjustments to differential extension caused by the slab tear, and probably also the strain partitioning between hot ductile lower crust driven by gravitational potential energy and the elastic response of an overlying thin brittle crust. These boundary conditions changed over time since the early Miocene.

7. Concluding remarks

Our fault-slip data provide an integrated, time-averaged record of brittle deformation along the diffuse Aegea-Anatolia plate-boundary zone from the Miocene to the present. They record different time intervals during the deformation of the Aegean-Anatolian continental crust. Comparing the brittle strain data with published geodetic and seismic data shows a relatively good but not perfect match for the present-day

Fig. 14. Summary map of all data in regional context. (a) Youngest extension directions from various data sets; note that recent extension directions from earthquake data (Fig. 1a) and velocity field (Fig. 1c) correspond with time-averaged directions from fault-slip data (fault-slip data from Sifnos (Ring et al., 2011) and Naxos (Ring et al., in preparation)). (b) Kinematic directions from fault-slip data for intermittent shortening phase with approximate age. (c) Earlier extensions directions derived from fault-slip data on high-angle faults (this study) and extension directions from low-angle extensional detachments (Thomson et al., 2009; Brichau et al., 2010; Jolivet and Brun, 2010; Ring et al., 2010; Grasemann et al., 2012); note that this extension phase shows more consistent NNE oriented directions than young extension phase, except for Samos Island; note limited match between extension direction from recent velocity field (Fig. 1c) and Miocene extension directions.

GPS motions. However, our data question the validity of extrapolating strain measurements of actively deforming regions to the protracted Miocene to recent deformation history of the Hellenic backarc.

We have identified two brittle deformation increments, a Pliocene to Recent crustal stretching increment with oblate strain geometry, and early to late Miocene extension partly accompanied by shortening resulting in prolate strain. The youngest fault increment is most readily comparable between the various areas and is associated with seismically active faults that control topography. In general, this youngest increment documents Pliocene to Recent NNE extension over large areas, but locally the extension direction can be SE (Amorgos and Astipalea Islands) and ESE (eastern Crete). We conclude that this regional complexity reflects a rather homogeneous regional 'background' NNE extension on which radial extension due to the increasing curvature of the Hellenic arc and possibly differential extension in a wrench corridor are superimposed.

Although older faulting increments are harder to compare because often only relative ages can be established, these older, Miocene (~24–5 Ma) fault-slip data suggest overall prolate strain geometry, where N–S stretching is locally accompanied by E–W shortening. On some islands, this shortening phase is short-lived and most likely did not occur at the same time across the study areas. Where shortening is accommodated by large-wavelength folding it appears to be an elastic response perpendicular to large-scale, highly ductile extension rather than being caused by far-field tectonic loading.

On Samos, Island early/middle Miocene extension is E–W directed, probably reflecting extension in a sinistral wrench corridor that formed in the early/mid Miocene. This sinistral wrench corridor of heterogeneous crustal deformation is spatially associated with uncharacteristically old fission track ages.

Overall NNE extension has been the dominant regime in the eastern Aegean since the early Miocene with intermittent phases of short-lived E–W shortening. Both the existence of a corridor of heterogeneous crustal deformation coincident with an area with an older cooling history, and the apparent change in strain geometry in time challenge concepts that assume, or propose, that the eastern Aegean Sea and western Anatolia have been deformed as a continuous tectonic domain since the Miocene.

Acknowledgements

Funded by the Deutsche Forschungsgemeinschaft (Ri 538/4 and Ri 538/18). We thank Hagen Deckert for various discussions and Bernhard Grasemann and an anonymous reviewer for commenting on the manuscript.

References

Aktug, B., et al., 2009. Deformation of western Turkey from a combination of permanent and campaign GPS data: limits to block-like behaviour. J. Geophys. Res. 114, B10404. http://dx.doi.org/10.1029/2008JB006000.

Altunkaynak, S., Rogers, N.W., Kelley, S.P., 2010. Causes and effects of geochemical variations in late Cenozoic volcanism of the Foça volcanic centre, NW Anatolia, Turkey. Int. Geol. Rev. 52:579–607. http://dx.doi.org/10.1080/00206810903360455.

Angelier, J., Lyberis, N., Le Pichon, X., Barrier, E., Huchon, P., 1982. The tectonic development of the Hellenic arc and the Sea of Crete: a synthesis. Tectonophysics 86, 159–196.

Avigad, D., Ziv, A., Garfunkel, Z., 2001. Ductile and brittle shortening, extension-parallel folds and maintenance of crustal thickness in the central Aegean. Tectonics 20, 277–287.

Axen, G.J., Selverstone, J., Byrne, T., Fletcher, J.M., 1998. If the strong crust leads, will the weak crust follow? GSA Today 8 (12), 1–8.

Bargnesi, E.A., Stockli, F., Mancktelow, N., Soukis, K., 2012. Miocene core complex development and coeval supradetachment basin evolution of Paros, Greece, insights from (U–Th)/He thermochronometry. Tectonophysics 595, 165–182.

Barka, A., 1992. The North Anatolian Fault Zone. Annal. Tecton. 6, 164–195.

Barka, A., Reilinger, R., 1997. Active tectonics of the Eastern Mediterranean region: deduced from GPS, neotectonic and seismicity data. Ann. Geofis. 40, 587–610.

Beaudoin, A., Laurent, V., Augier, R., Rabillard, A., Jolivet, L., Arbaret, L., Menant, A., 2015. The Ikaria metamorphic core complex between the Cyclades and the Menderes Massif. J. Geodyn. 92, 18–41.

Benetatos, C., Kiratzi, A., Papazachos, C., Karakaisis, G., 2004. Focal mechanisms of shallow and intermediate depth earthquakes along Hellenic Arc. J. Geodyn. 37, 253–296.

Berger, A., Schneider, D.A., Grasemann, B., Stockli, D., 2013. Footwall mineralization during Late Miocene extension along the West Cycladic Detachment System, Lavrion, Greece. Terra Nova 25, 181–191.

Berk Biryol, C., Beck, S.L., Zandt, G., Özacar, A.A., 2011. Segmented African lithosphere beneath the Anatolian region inferred from teleseismic P-wave tomography. Geophys. J. Int. 184, 1037–1057.

Billiris, H., Pardissis, D., Veis, G., et al., 1991. Geodetic determination of tectonic deformation in Central Greece from 1900 to 1988. Nature 350, 124–129.

Bohnhoff, M., Rische, M., Meier, T., Becker, D., Stavrakakis, G., Harjes, H.-P., 2006. Microseismic activity in the Hellenic volcanic arc, Greece, with emphasis on the seismotectonic setting of the Santorini-Amorgos zone. Tectonophysics 423, 17–33.

Bolhar, R., Ring, U., Allen, C.M., 2010. An integrated zircon geochronological and geochemical investigation into the Miocene plutonic evolution of the Cyclades, Aegean Sea, Greece: part 1—geochronology. Contrib. Mineral. Petrol. 160:719–742. http://dx.doi.org/10.1007/s00410-010-0504-4.

Bolhar, R., Ring, U., Ireland, T.I., 2017. Zircon in amphibolites from Naxos, Aegean Sea, Greece: origin, significance and tectonic setting. J. Metamorph. Geol. 36. http://dx.doi.org/10.1111/jmg.12238.

de Boorder, H., Spakman, W., White, S.H., Wortel, M.J.R., 1999. Late Cenozoic mineralization, orogenic collapse and slab detachment in the European Alpine Belt. Earth Planet. Sci. Lett. 164, 569–575.

Brichau, S., Ring, U., Carter, A., Bolhar, R., Monie, P., et al., 2008. Timing, slip rate, displacement and cooling history of the Mykonos detachment footwall, Cyclades, Greece, and implications for the opening of the Aegean Sea basin. J. Geol. Soc. Lond. 165, 263–277.

Brichau, S., Ring, U., Ketcham, R.A., Carter, A., Stockli, D., Brunel, M., 2006. Constraining the long-term evolution of the slip rate for a major extensional fault system in the central Aegean, Greece, using thermochronology. Earth Planet. Sci. Lett. 241:293–306. http://dx.doi.org/10.1016/j.epsl.2005.09.065.

Brichau, S., Ring, U., Carter, A., Monie, P., Bolhar, R., et al., 2007. Extensional faulting on Tinos Island, Aegean Sea, Greece: how many detachments? Tectonics 26, TC4009. http://dx.doi.org/10.1029/2006TC001969.

Brichau, S., Thomson, S., Ring, U., 2010. Thermochronometric constraints on the tectonic evolution of the Serifos detachment, Aegean Sea, Greece. Int. J. Earth Sci. 99, 379–393.

Brix, M.R., Stöckhert, B., Seidel, E., Theye, T., Thomson, S.N., Küster, M., 2002. Thermobarometric data from a fossil zircon partial annealing zone in high pressure–low temperature rocks of eastern and central Crete, Greece. Tectonophysics 349, 309–326.

Buick, I.S., Holland, T.J.B., 1989. The P-T-t path associated with crustal extension, Naxos, Cyclades, Greece. Geol. Soc. Lond., Spec. Publ. 43:365–369. http://dx.doi.org/10.1144/GSL.SP.1989.043.01.32.

Buscher, J.T., Hampel, A., Hetzel, R., Dunkl, I., Glotzbach, C., Struffert, A., Akal, C., Rätz, M., 2013. Quantifying rates of detachment faulting and erosion in the central Menderes Massif (western Turkey) by thermochronology and cosmogenic 10Be. J. Geol. Soc. Lond. 170:669–683. http://dx.doi.org/10.1144/jgs2012-132.

Caputo, R., Catalano, S., Monaco, C., Romagnoli, G., Tortorici, G., Tortorici, L., 2010. Active faulting on the island of Crete (Greece). Geophys. J. Int. 183, 111–126.

Cemen, I., Catlos, E.J., Gögüs, O., Özerdem, C., 2006. Postcollisional extensional tectonics and exhumation of the Menderes Massif in the Western Anatolia extended terrane, Turkey. In: Dilek, Y., Pavlides, S. (Eds.), Postcollisional Tectonics and Magmatism in the Mediterranean Region and Asia. Geol. Soc. Am. Spec. Pap Vol. 409, pp. 353–379.

Chatzaras, P., Xypolias, P., Kokkalas, S., Koukouvelas, I., 2011. Oligocene–Miocene thrusting in central Aegean: insights from the Cycladic island of Amorgos. Geol. J. 46, 619–636.

Creutzburg, N., et al., 1977. General geological map of Greece. Crete Island 1:200 000. Athens, Institute of Geological and Mining Research.

Davies, R., England, P., Parsons, B., et al., 1997. Geodetic strain of Greece in the interval 1892–1992. J. Geophys. Res. B102, 24571–24588.

Dimitriadis, I., Karagianni, E., Panagiotopoulos, D., Papazachos, C., Hatzidimitriou, P., Bohnhoff, M., Rische, M., Meier, T., 2009. Seismicity and active tectonics at Coloumbo reef (Aegean Sea, Greece): monitoring an active volcano at Santorini volcanic center using a temporary seismic network. Tectonophysics 465, 136–149.

Duretz, T., Gerya, T., Spakman, W., 2014. Slab detachment in laterally varying sub-duction zones: 3D numerical modeling. Geophys. Res. Lett. 41:1951–1956. http://dx.doi.org/10.1002/2014GL059472.

Emre, O., Barka, A., 2000. Active faults between Gediz graben and Aegean sea (Izmir region). Proceedings of International Symposia on Seismicity of Western Anatolia, Turkey.

Fassoulas, C., 2001. The tectonic development of a Neogene basin at the leading edge of the active European margin: the Heraklion basin, Crete, Greece. J. Geodyn. 31, 49–70.

Fassoulas, C., Kilias, A., Mountrakis, D., 1994. Postnappe stacking extension and exhumation of high-pressure/low-temperature rocks in the island of Crete, Greece. Tectonics 13, 127–138.

Friedrich, W., Brüstle, A., Küperkoch, L., Meier, T., Lamara, S., Egelados Working Group, 2014. Focal mechanisms and stress field in the southern Aegean. Solid Earth 5, 275–297.

Gallen, S.F., Wegmann, K.W., Bohnenstiehl, D.R., Pazzaglia, F.J., Brandon, M.T., Fassoulas, C., 2014. Active simultaneous uplift and margin-normal extension in a forearc high, Crete, Greece. Earth Planet. Sci. Lett. 398, 11–24.

Ganas, A., Parsons, T., 2009. Three-dimensional model of Hellenic arc deformation and origin of the Cretan uplift. J. Geophys. Res. 114, B06404. http://dx.doi.org/10.1029/2008JB005599.

Ganas, A., Pavildes, S., Karastathis, V., 2005. DEM-based morphometry of range-front escarpments in Attica, Central Greece, and its relation to fault slip rates. Geomorphology 65, 301–319.
Genç, C., Altunkaynak, S., Karacik, Z., Yazman, M., Yilmaz, Y., 2001. The Cubuklu graben, south of Izmir: tectonic significance in the Neogene geological evolution of the western Anatolia. Geodin. Acta 14, 45–55.
Gessner, K., Ring, U., Johnson, C., Hetzel, R., Passchier, C.W., Güngör, T., 2001. An active bivergent rolling-hinge detachment system: the central Menderes metamorphic core complex in western Turkey. Geology 29, 611–614.
Gessner, K., Ring, U., Güngör, T., 2011. Along-strike variations in the eastern Mediterranean Tethyan orogen: Field guide to Samos and the Menders Massif. Geol. Soc. Am., Field Trip Guide 23.
Gessner, K., Gallardo, L.A., Markwitz, V., Ring, U., Thomson, S.T., 2013. What caused the denudation of the Menderes massif: review of crustal evolution, lithosphere structure, and dynamic topography in southwest Turkey. Gondwana Res. 24:243–274. http://dx.doi.org/10.1016/j.gr.2013.1001.1005.
Gessner, K., Gallardo, L., Wedin, F., Sener, A., 2016. Crustal structure of the northern Menderes Massif, western Turkey, imaged by joint gravity and magnetic inversion. Int. J. Earth Sci. 105, 2133–2148.
Govers, R., Wortel, M.J.R., 2005. Lithosphere tearing at STEP faults: response to edges of subduction zones. Earth Planet. Sci. Lett. 236, 505–523.
Grasemann, B., Schneider, D.A., Stöckli, D.F., Iglseder, C., 2012. Miocene bivergent crustal extension in the Aegean: evidence from the western Cyclades (Greece). Lithosphere 4:23–39. http://dx.doi.org/10.1130/L164.1.
Hejl, E., Riedl, H., Weingartner, H., 2002. Post-plutonic unroofing and morphogenesis of the Attic-Cycladic complex (Aegea, Greece). Tectonophysics 349, 37–56.
Hetzel, R., Ring, U., Akal, C., Troesch, M., 1995. Miocene NNE-directed extensional unroofing in the Menderes massif, southwestern Turkey. J. Geol. Soc. Lond. 152, 639–654.
Hetzel, R., Zwingmann, H., Mulch, A., Gessner, K., Akal, C., Hampel, A., Güngör, T., Petschick, R., Mikes, T., Wedin, F., 2013. Spatio-temporal evolution of brittle normal faulting and fluid infiltration in detachment fault systems — a case study from the Menderes Massif, western Turkey. Tectonics 32:364–376. http://dx.doi.org/10.1002/tect.20031.
van Hinsbergen, D.J.J., Meulenkamp, J.E., 2006. Neogene supradetachment basin development on Crete (Greece) during exhumation of the South Aegean core complex. Basin Res. 18, 103–124.
van Hinsbergen, D.J.J., 2010. A key extensional metamorphic complex reviewed and restored: the Menderes massif of western Turkey. Earth Sci. Rev. 102, 60–76.
Işık, V., Tekeli, O., 2001. Late orogenic crustal extension in the northern Menderes massif (western Turkey): evidence for metamorphic core complex formation. Int. J. Earth Sci. 89, 757–765.
Jackson, J., McKenzie, D., 1988. The relationship between plate motions and seismic moment tensors, and rates of active deformation in the Mediterranean and Middle East. Geophys. J. Int. 93, 45–73.
Jansen, J.B.H., Schuiling, R.D., 1976. Metamorphism on Naxos: petrology and geothermal gradients. Am. J. Sci. 276, 1225–1253.
Jolivet, L., Brun, J.P., 2010. Cenozoic geodynamic evolution of the Aegean. Int. J. Earth Sci. 99:109–138. http://dx.doi.org/10.1007/s00531-008-0366-4.
Jolivet, L., Menant, A., Sternai, P., Rabillard, A., Arbaret, L., Augier, A., Laurent, V., Beaudoin, A., Grasemann, B., Huet, B., Labrousse, L., Le Pourhiet, L., 2015. The geological signature of a slab tear below the Aegean. Tectonophysics 659, 166–182.
Kahle, H.G., Cocard, R., Peter, Y., Geiger, A., Reilinger, R., et al., 1999. The GPS strain rate field in the Aegean Sea and western Anatolia. Geophys. Res. Lett. 26, 2513–2516.
Kincaid, C., Griffiths, R.W., 2004. Variability in flow and temperatures within mantle subduction zones. Geochem. Geophys. Geosyst. 5, 458–472.
Kiratzi, A.A., Louvari, E., 2003. Focal mechanisms of shallow earthquakes in the Aegean Sea and the surrounding lands determined by waveform modelling: a new database. J. Geodyn. 36, 251–274.
Kiratzi, A.A., Papazachos, C.B., 1995. Active seismic deformation in the southern Aegean Benioff zone. J. Geodyn. 19, 65–78.
Kopf, A., Mascle, J., Klaeschen, D., 2003. The Mediterranean Ridge: a mass balance across the fastest growing accretionary complex on Earth. J. Geophys. Res. B108, 2372–2399.
Kumerics, C., Ring, U., Brichau, S., Glodny, J., Monie, P., 2005. The extensional Messaria shear zone and associated brittle detachment faults, Aegean Sea, Greece. J. Geol. Soc. Lond. 162, 701–721.
Laws, S., Bernet, M., Zahid, M., Ring, U., 1997. Die tektonische Entwicklung der Insel Samos (östliche Ägäis): extensionstransfer zwischen den Kykladen und dem Menderes Massif? Zbl. Geol. Paläontol. 3, 109–112.
Le Pichon, X., Angelier, J., 1981. The Aegean Sea. Phil. Trans. R. Soc. Lond. 300, 357–372.
Le Pichon, X., Kreemer, C., 2010. The Miocene-to-present kinematic evolution of the eastern Mediterranean and Middle East and its implications for dynamics. Annu. Rev. Earth Planet. Sci. 38:323–351. http://dx.doi.org/10.1146/annurev-earth-040809-152419.
Le Pichon, X., Chamot-Rooke, N., Lallemant, S., Noomen, R., Veis, G., 1995. Geodetic determination of the kinematics of central Greece with respect to Europe: implications for eastern Mediterranean tectonics. J. Geophys. Res. 100, 12675–12690.
Lévy, F., Jaupart, C., 2011. Folding in regions of extension. Geophys. J. Int. 185, 1120–1134.
Linnros, H., 2016. A 3-dimensional Tectonic Model of the Naxos Metamorphic Core Complex, Greece. Masters thesis. Stockholm University.
Mardia, K.V., 1972. Statistics of Directional Data. Academic Press, London.
Marrett, R., Allmendinger, R.W., 1990. Kinematic analysis of fault-slip data. J. Struct. Geol. 12, 973–986.
Marsellos, A.E., Kidd, W.S.F., 2008. Extension and exhumation of the Hellenic forearc ridge in Kythera. J. Geol. 116, 640–649.
Marsellos, A.E., Kidd, W.S.F., Garver, J.I., Kyriakopoulos, K.G., 2012. Exhumation of HP-rocks accompanied by low-angle normal faulting and associated detachment fault of Milos Island - evidence from zircon fission-track thermochronology. Contrib. Mineral. Petrol. 49, 46–49.
Martin, L., Duchêne, S., Deloule, E., Vanderhaeghe, O., 2006. The isotopic composition of zircon and garnet: a record of the metamorphic history of Naxos, Greece. Lithos 87: 174–192. http://dx.doi.org/10.1016/j.lithos.2005.06.016.
McClusky, S., Balassanian, S., Barka, A., Demir, C., Ergintasv, S., Georgiev, I., Gurkan, O., Hamburger, M., Hurst, K., Kahle, H., Kastens, K., Kekelidze, G., King, R., Kotzev, V., Lenk, O., Mahmoud, S., Mishin, A., Nadariya, M., Ouzounis, A., Paradisssis, D., Peter, Y., Prilepin, M., Reilinger, R., Sanli, I., Seeger, H., Tealeb, A., Toksoz, M.N., Veis, G., 2000. Global positioning system constraints on plate kinematics and dynamics in the Eastern Mediterranean and Caucasus. J. Geophys. Res. 105, 5695–5719.
McKenzie, D.P., 1978. Active tectonics of the Alpine-Himalayan belt: the Aegean Sea and surrounding regions. Geophys. J. R. Asstr. Soc. 55, 217–354.
Menant, A., Jolivet, L., Augier, R., Skarpelis, N., 2013. The North Cycladic Detachment System and associated mineralization, Mykonos, Greece: insights on the evolution of the Aegean domain. Tectonics 32:433–452. http://dx.doi.org/10.1002/tect.20037.
Mercier, J.L., 1981. Extensional-compressional tectonics associated with the Aegean arc: comparison with the Andean Cordillera of south Peru-north Bolivia. Philos. Trans. R. Soc. 300, 337–355.
Mercier, J.L., Sorel, D., Vergely, P., Simeakis, K., 1987. Extensional tectonic regimes in the Aegean basins during the Cenozoic. Basin Res. 2, 49–71.
Micheuz, P., Krenn, M., Fritz, H., Kurz, W., 2015. Tectonometamorphic evolution of blueschist-facies rocks in the phyllite-quartzite unit of the external Hellenides (Mani, Greece). Austrian Journal of Earth Sciences 108, 312–342.
Moresi, L., Betts, P.G., Miller, M.S., Cayley, R.A., 2015. Dynamics of continental accretion. Nature 508:244–248. http://dx.doi.org/10.1038/nature13033.
Özeren, M.S., Holt, W.E., 2010. The dynamics of the eastern Mediterranean and eastern Turkey. Geophys. J. Int. 183:1165–1184. http://dx.doi.org/10.1111/j.1365-246X.2010.04819.x.
Özkaymak, C., Sözbilir, H., Uzel, B., 2013. Neogene-quaternary evolution of the Manisa Basin: evidence for variation in the stress pattern of the Izmir-Balıkesir transfer zone, western Anatolia. J. Geodyn. 65, 117–135.
Papadopoulos, G.A., Pavlides, S.B., 1992. The large 1956 earthquake in the South Aegean: macroseismic field configuration, faulting and neotectonics of Amorgos island. Earth Planet. Sci. Lett. 113, 383–396.
Papazachos, B.C., Karakostas, V.G., Papazachos, C.B., Scordilis, E.M., 2000. The geometry of the Wadati–Benioff zone and lithospheric kinematics in the Hellenic arc. Tectonophysics 319, 275–300.
Pe-Piper, G., Piper, D.J.W., 2007. Late Miocene igneous rocks of Samos: the role of tectonism in petrogenesis in the southeastern Aegean. Geol. Soc. Lond. Spec. Publ. 291, 75–97.
Pérouse, E., Chamot-Rooke, N., Rabaute, A., Briole, P., Jouanne, F., Georgiev, I., Dimitrov, D., 2012. Bridging onshore and offshore present-day kinematics of central and eastern Mediterranean: implications for crustal dynamics and mantle flow. Geochem. Geophys. Geosyst. 13, 678–693, Q09013.
Petit, J.-P., 1987. Criteria for the sense of movement on fault surfaces in brittle rocks. J. Struct. Geol. 9, 597–608.
Piromallo, C., Becker, T.W., Funiciello, F., Faccenna, C., 2006. Three-dimensional instantaneous mantle flow induced by subduction. Geophys. Res. Lett. 33, L08304. http://dx.doi.org/10.1029/2005GL025390.
Prelevic, D., Akal, C., Romer, R.L., Foley, S.F., 2010. Lamproites as indicators of accretion and/or shallow subduction in the assembly of south-western Anatolia, Turkey. Terra Nova 22, 443–452.
Purvis, M., Robertson, A., 2004. A pulsed extension model for the Neogene–recent E–W trending Alasehir graben and the NE–SW-trending Selendi and Gordes basins, western Turkey. Tectonophysics 391, 171–201.
Purvis, M., Robertson, A., 2005. Miocene sedimentary evolution of the NE–SW-trending Selendi and Gordes basins, W Turkey: implications for extensional processes. Sediment. Geol. 174, 31–62.
Rabillard, A., Arbaret, L., Jolivet, L., et al., 2015. Interactions between plutonism and detachments during metamorphic core complex formation, Serifos Island (Cyclades, Greece). Tectonics 34, 1080–1106.
Reilinger, R., et al., 1997. Global positioning system measurements of present-day crustal movements in the Arabia–Africa–Eurasia plate collision zone. J. Geophys. Res. 102, 9983–9999.
Reilinger, R., McClusky, S., Vernant, P., Lawrence, S., Ergintav, S., Cakmak, R., Ozener, H., Kadirov, F., Guliev, I., Stepanyan, R., Nadariya, M., Hahubia, G., Mahmoud, S., Sakr, K., ArRajehi, A., Paradissis, D., Al-Aydrus, A., Prilepin, M., Guseva, T., Evren, E., Dmitrotsa, A., Filikov, S.V., Gomez, F., Al-Ghazzi, R., Karam, G., 2006. GPS constraints on continental deformation in the Africa-Arabia-Eurasia continental collision zone and implications for the dynamics of plate interactions. J. Geophys. Res. 111, 9856–9879, B05411.
Reiners, P.W., Brandon, M.T., 2006. Using thermochronology to understand orogenic erosion. Annu. Rev. Earth Planet. Sci. 34, 419–466.
Ring, U., 2001. Structure and deformation history of Astypalea Island, Aegean Sea. Bull. Geol. Soc. Greece 34, 329–335.
Ring, U., Collins, A.S., 2005. SHRIMP dating of the syn-tectonic Egrigöz granite: precise timing of core-complex formation in the Anatolide belt of western Turkey. J. Geol. Soc. Lond. 162, 289–298.
Ring, U., Laws, S., Bernet, M., 1999. Structural analysis of a complex nappe sequence and late-orogenic basins from the Aegean Samos Island, Greece. J. Struct. Geol. 21: 1575–1601. http://dx.doi.org/10.1016/S0191-8141(99)00108-X.

Ring, U., Brachert, T., Fassoulas, C., 2001. Middle Miocene graben development in Crete and its possible relation to large-scale detachment faults. Terra Nova 13, 297–304.

Ring, U., Johnson, C., Hetzel, R., Gessner, K., 2003a. Tectonic denudation of a Late Cretaceous–Tertiary collisional belt: regionally symmetric cooling patterns and their relation to extensional faults in the Anatolide belt of western Turkey. Geol. Mag. 140, 421–441.

Ring, U., Brachert, T.C., ten Veen, J.H., Kleinspehn, K.L., 2003b. Discussion on incipient continental collision and plate-boundary curvature: Late Pliocene-Holocene transtensional Hellenic forearc, Crete, Greece. J. Geol. Soc. 160, 819–824.

Ring, U., Will, T., Glodny, J., Kumerics, C., Gessner, K., Thomson, S.N., Güngür, T., Monie, P., Okrusch, M., Drüppel, K., 2007a. Early exhumation of high-pressure rocks in extrusion wedges: the Cycladic blueschist unit in the eastern Aegean, Greece and Turkey. Tectonics 26, TC2001. http://dx.doi.org/10.1029/2005TC001872.

Ring, U., Glodny, J., Will, T., Thomson, S., 2007b. An Oligocene extrusion wedge of blueschist-facies nappes on Evia, Aegean Sea, Greece: implications for the early exhumation of high-pressure rocks. J. Geol. Soc. Lond. 164:637–652. http://dx.doi.org/10.1144/0016-76492006-041.

Ring, U., Thomson, S.N., Rosenbaum, G., 2009. Timing of the Amorgos detachment system and implications for detachment faulting in the southern Aegean Sea, Greece. Geol. Soc. Lond. Spec. Publ. 321:169–178. http://dx.doi.org/10.1144/SP321.8.

Ring, U., Glodny, J., Will, T., Thomson, S., 2010. The Hellenic subduction system: high-pressure metamorphism, exhumation, normal faulting, and large-scale extension. Annu. Rev. Earth Planet. Sci. 38:45–76. http://dx.doi.org/10.1146/annurev.earth.050708.170910.

Ring, U., Glodny, J., Will, T., Thomson, S.N., 2011. Normal faulting on Sifnos Island and the South Cyclades Detachment System, Aegean Sea, Greece. J. Geol. Soc. Lond. 168: 751–768. http://dx.doi.org/10.1144/0016-76492010-064.

Ring, U., Thomson, S.H., Gessner, K., 2017. The south Menderes monocline in the southern Anatolide belt of west Turkey. J. Geol. Soc. Lond. (in preparation).

Roberts, G.P., Ganas, A., 2000. Fault-slip directions in central and southern Greece measured from striated and corrugated fault planes: comparison with focal mechanism and geodetic data. J. Geophys. Res. 105:443–423,462. http://dx.doi.org/10.1029/1999JB900440.

Rosenbaum, G., Ring, U., 2007. Structure and metamorphism of Amorgos: a field excursion. In: Lister, G., Forster, M., Ring, U. (Eds.), Inside the Aegean Metamorphic Core Complexes. J. Virt. Expl., Electronic Edition, ISSN Vol. 28, pp. 1441–8142 (Paper 7).

Rosenbaum, G., Ring, U., Kühn, A., 2007. Tectono-metamorphic evolution of high-pressure rocks from the island of Amorgos (Central Aegean, Greece). J. Geol. Soc. Lond. 164, 425–438.

Royden, L.H., 1993. Evolution of retreating subduction boundaries formed during continental collision. Tectonics 12, 629–638.

Ryan, W.B.F., Carbotte, S.M., Coplan, J.O., O'Hara, S., Melkonian, A., Arko, R., Weissel, R.A., Ferrini, V., Goodwillie, A., Nitsche, F., Bonczkowski, J., Zemsky, R., 2009. Global multi-resolution topography synthesis. Geochem. Geophys. Geosyst. 10, Q03014. http://dx.doi.org/10.1029/2008GC002332.

Seidel, M., Seidel, E., Stöckhert, B., 2007. Tectono-sedimentary evolution of lower to middle Miocene half-graben basins related to an extensional detachment fault (western Crete, Greece). Terra Nova 19, 39–47.

Şengör, A.M.C., Yilmaz, Y., 1981. Tethyan evolution of Turkey: a plate tectonic approach. Tectonophysics 75, 181–241.

Şengör, A.M.C., Satir, M., Akkök, R., 1984. Timing of tectonic events in the Menderes Massif, western Turkey: implications for tectonic evolution and evidence for Pan-African basement in Turkey. Tectonics 3, 693–707.

Şengör, A.M.C., Özeren, S., Genç, T., Zor, E., 2003. East Anatolian high plateau as a mantle supported, north–south shortened domal structure. Geophys. Res. Lett. 30, 8045–8049.

Şengör, A.M.C., Özeren, M.S., Keskin, M., Sakınç, M., Özbakır, A.D., Kayan, G., 2008. Eastern Turkish high plateau as a small Turkish-type orogen: implications for post-collisional crust forming processes in Turkish-type orogens. Earth Sci. Rev. 90, 1–48.

Seward, D., Vanderhaeghe, O., Siebenaller, L., Thomson, S., Hibsch, C., Zingg, A., Holzner, P., Ring, U., Duchene, S., 2009. Cenozoic tectonic evolution of Naxos Island through a multi-faceted approach of fission-track analysis. Geol. Soc. Lond. Spec. Publ. 321: 179–196. http://dx.doi.org/10.1144/SP321.9.

Seyitoğlu, G., Tekeli, O., Cemen, I., Sen, S., Isık, V., 2002. The role of flexural rotation/rolling hinge model in the tectonic evolution of the Alasehir Graben, western Turkey. Geol. Mag. 139, 15–26.

Seyitoğlu, G., Isik, V., Çemen, I., 2004. Complete tertiary exhumation history of the Menderes Massif, western Turkey: an alternative working hypothesis. Terra Nova 16: 358–364. http://dx.doi.org/10.1111/j.1365-3121.2004.00574.x.

Sodoudi, F., Kind, R., Hatzfeld, D., Priestley, K.F., Hanka, W., Wylegalla, K., Stavrakakis, G., Vafidis, A., Harjes, H.-P., Bohnhoff, M., 2006. Lithospheric structure of the Aegean obtained from P and S receiver functions. J. Geophys. Res. 111, B12307.

Stiros, S.C., Marangou, L., Arnold, M., 1994. Quaternary uplift and tilting of Amorgos Island (southern Aegean) and the 1956 earthquake. Earth Planet. Sci. Lett. 128, 65–76.

Sümer, Ö., Inci, U., Sözbilir, H., 2013. Tectonic evolution of the Söke Basin: extension-dominated transtensional basin formation in western part of the Büyük Menderes Graben, western Anatolia, Turkey. J. Geodyn. 65, 148–175.

Tan, O., Tapırdamaz, C., Yrük, A., 2008. The earthquake catalogues for Turkey. Turk. J. Earth Sci. 17, 405–418.

Tan, O., Papadimitriou, E.E., Pabuccu, Z., Karakostas, V., Yörük, A., Leptokaropoulos, K., 2014. A detailed analysis of microseismicity in Samos and Kusadasi (Eastern Aegean Sea) areas. Acta Geotech. 62, 1283–1309.

Thomson, S.N., Ring, U., 2006. Thermochronologic evaluation of post-collision extension in the Anatolide Orogen, western Turkey. Tectonics 25, TC3005.

Thomson, S.N., Stöckhert, B., Brix, M.R., 1998a. Thermochronology of the high-pressure metamorphic rocks of Crete, Greece: implications for the speed of tectonic processes. Geology 26, 259–262.

Thomson, S.N., Stöckhert, B., Rauche, H., Brix, M.R., 1998b. Apatite fission-track thermochronology of the uppermost tectonic unit of Crete, Greece: implications for the post-Eocene tectonic evolution of the Hellenic Subduction System. In: Van den Haute, P., De Corte, F. (Eds.), Advances in Fission-Track Geochronology. Kluwer Acad, Dordrecht, The Netherlands, pp. 187–205.

Thomson, S.N., Stöckhert, B., Brix, M.R., 1999. Miocene high-pressure metamorphic rocks of Crete, Greece: rapid exhumation by buoyant escape. Geol. Soc. Lond. Spec. Publ. 154, 87–108.

Thomson, S.N., Ring, U., Brichau, S., Glodny, J., Will, T.M., 2009. Timing and nature of formation of the Ios metamorphic core complex, southern Cyclades, Greece. Geol. Soc. Lond. Spec. Publ. 321, 139–167.

Uzel, B., Sözbilir, H., Özkaymak, C., 2012. Neotectonic evolution of an actively growing superimposed basin in western Anatolia: the inner bay of Izmir, Turkey. Turk. J. Earth Sci. 21, 439–471.

Venkat-Ramani, M., Tikoff, B., 2002. Physical models of transtensional folding. Geology 30, 523–526.

Wijbrans, J.R., McDougall, I., 1988. Metamorphic evolution of the Attic Cycladic Metamorphic Belt on Naxos (Cyclades, Greece) utilizing $^{40}Ar/^{39}Ar$ age spectrum measurements. J. Metamorph. Geol. 6, 571–594.

Wijns, C., Weinberg, R., Gessner, K., Moresi, L., 2005. Mode of crustal extension determined by rheological layering. Earth Planet. Sci. Lett. 236, 120–134.

Wyers, G.P., 1987. Petrogenesis of Calc-alkaline and Alkaline Magmas From the Southern and Eastern Aegean Sea, Greece. Ph.D. Thesis. The Ohio State University.

Wyers, G.P., Barton, M., 1986. Petrology and evolution of transitional alkaline-sub-alkaline lavas from Patmos, Greece: evidence for fractional crystallization, magma mixing and assimilation. Contrib. Mineral. Petrol. 93, 297–311.

Wyers, G.P., Barton, M., 1987. Geochemistry of a transitional ne-trachybasalt - Q-trachyte lava series from Patmos (Dodecanesos), Greece: further evidence for fractionation, mixing and assimilation. Contrib. Mineral. Petrol. 97, 279–291.

Yilmaz, Y., Genç, S.C., Gürer, F., Bozcu, M., Yilmaz, K., Karacik, Z., Altunkayak, S., Elmas, A., 2000. When did the western Anatolian grabens begin to develop? In: Bozkurt, E., Winchester, J.A., Piper, J.D.A. (Eds.), Tectonics and Magmatism in Turkey and the Surrounding Area, pp. 353–384

Yolsal-Çevikbilen, S., Taymaz, T., Helvacı, C., 2014. Earthquake mechanisms in the Gulfs of Gökova, Sığacık, Kuşadası, and the Simav Region (western Turkey): neotectonics, seismotectonics and geodynamic implications. Tectonophysics 635, 100–124.